4

Results and Discussion

The study employed a comprehensive approach, including pharmacognostic study, phytochemical analysis, antioxidant assessments, *in vitro* and *in vivo* evaluations of antiurolithiasis activity. Chromatography and *in silico* studies further validated the SASM extract's potential.

PHASE I

4.1 Phytochemical Screening and Antioxidant Activities of *S. articularis* L.f.

4.1.1 Pharmacognostic Study

4.1.1.1 Organoleptic Study

4.1.1.2 Fluorescence Analysis

4.1.2. Qualitative Analysis of Phytochemicals

4.1.3 Quantification of Phytochemical Constituents

4.1.3.1 Estimation of Primary Metabolites

4.1.3.2 Estimation of Secondary Metabolites

4.1.4 Evaluation of Antioxidant Activity

4.1.4.1 Estimation of Enzymatic Antioxidants

4.1.4.2 Estimation of Non-Enzymatic Antioxidants

4.1.4.2.1 Estimation of Total Phenolic Content

4.1.4.2.2 Estimation of Total Flavonoid Content

4.1.4.2.3 Estimation of Ascorbic Acid and Alpha-Tocopherol

4.1.5 *In vitro* Radical Scavenging Assay

4.1.5.1 DPPH Radical Scavenging Assay

4.1.5.2 Ferric Reducing Antioxidant Power Assay

4.1.5.3 ABTS Radical Scavenging Assay

PHASE II

4.2 Antiurolithiatic Activity of *Spermacoce articularis*

4.2.1 *In vitro* Antiurolithiatic Activity

4.2.1.1 Effect of *S. articularis* Leaf Ethanol Extract on Calcium Oxalate Crystal Nucleation

4.2.1.2. Effect of *S. articularis* Stem Methanol (SASM) Extract on Calcium Oxalate Crystal Nucleation

4.2.1.3 Effect of *S. articularis* Leaf Ethanol and Stem Methanol Extract on Calcium Oxalate Crystal Aggregation

4.2.2 *In vivo* Antiurolithiatic Activity

4.2.2.1 Effect of SASM Extract on Different Urine Analysis Parameters

4.2.2.2 Effect of SASM Extract on Different Parameters of Serum and Hematology

4.2.2.3 Effect of SASM Extract on Animal Body and Kidney Weight

4.2.2.4 Effect of SASM on Different Antioxidant Parameters

4.2.2.5 Histopathological Analysis of Kidney at 400X

4.2.3 *In vitro* Cytotoxicity Assay of SASM Extract

4.2.3.1. Brine Shrimp Lethality Assay

4.2.3.2 Cytotoxic Properties of SASM Extract Against Kidney HEK 293 Cell Line

PHASE III

4.3 Chromatographic Profiling

4.3.1. Thin Layer Chromatographic Analysis

4.3.2. High-Performance Thin Layer Chromatographic Analysis

4.3.2.1 HPTLC Profiling for Terpenoids

4.3.2.2 HPTLC Profiling for Phenolics

4.3.3. Gas Chromatographic-Mass Spectrometry Analysis

PHASE IV

4.4 *In silico* Analysis of Anti-Urolithiatic Activity

4.4.1 Molecular Docking Studies Against Urolithiasis Receptors

4.4.2 Molecular Dynamics Simulation

4.4.3 The Pharmacokinetic Parameters and Drug Likeness of the Identified Compounds

PHASE I

4.1 Phytochemical Screening and Antioxidant Activities of *S. articularis*

Different extracts of *S. articularis* were screened and quantified for their bioactive compounds and evaluated for their antioxidant properties. The results pertaining to this study are reported and discussed below.

4.1.1 Pharmacognostic Study

Pharmacognostic study assesses physical, chemical, and biological properties of medicinal plant material for its quality and authenticity.

4.1.1.1 Organoleptic Study

The organoleptic evaluation revealed distinct characteristics among the leaf, stem, and root of the *S. articularis* fresh and powdered samples. The leaf and stem exhibited a green color, while the root displayed a brown hue. All three samples emitted a pleasant odor. The taste varied, the leaf and root possessed a bitter flavor, whereas the stem powder was tasteless. Organoleptic analysis provides a simple, rapid, and reliable preliminary tool for authenticating crude plant drugs. The results observed for organoleptic characters are noted in **Table 4.1**.

Table 4.1 Organoleptic study of *S. articularis*

Samples	Colour	Odour	Taste
Leaf	Dark green	Pleasant	Bitter
Stem	Olive green	Pleasant	Tasteless
Root	Light Brown	Pleasant	Bitter

4.1.1.2 Fluorescence Analysis

Fluorescence study is a crucial parameter for the initial standardization of crude drugs. The emitted light always has a longer wavelength than the excitation light. Short-wavelength light, such as ultraviolet light, is highly effective in inducing fluorescence in substances that do not visibly fluoresce under daylight (Kumar *et al*., 2012). The plant powders were treated with various solvents (water, acid, and alkali) and observed under both UV and visible light. Under treatment, the powder samples expressed different shades of colours like green, brown, yellow, and

black, which represent the purity of the plant materials, and the results were presented in Table **4.2.**

Table 4.2. Fluorescence analysis of *S. articularis* leaf, stem, and root powders

Treatment with chemical reagents	STEM			LEAF			ROOT		
	Visible Light	UV-Shortwave (254 nm)	UV- Longwave (365 nm)	Visible Light	UV-Short wave (254 nm)	UV-Longwave (365 nm)	Visible Light	UV - Short wave (254 nm)	UV-Longwave (365 nm)
Crude powder	Greenish brown	Dark brown	Light green	Dark green	Blackish green	Light green	Brown	Brown	Dark green
Powder with 1N HCL	Brown	Dark green	Light green	Dark green	Blackish green	Green	Dark Brown	Dark green	Dark green
Powder with 1N NaOH in methanol	Greenish brown	Green	Fluorescent green	Green	Dark green	Light green	Yellowish brown	Dark green	Dark green
Powder with 50% HNO_3	Light brown	Yellowish green	Fluorescent green	Brownish	Blackish green	Green	Brown	Blackish green	Dark green
Powder with acetic acid	Brown	Dark green	Fluorescent green	Yellowish green	Blackish green	Fluorescent green	Dark brown	Black	Blackish green
Powder with picric acid	Yellowish green	Fluorescent green	High fluorescent green	Fluorescent green	Yellowish green	Fluorescent green	Fluorescent yellow	Fluorescent green	Fluorescent light green
Powder + 1% $Fecl_3$	Greenish black	Greenish black	Dark green	Dark green	Blackish green	Yellowish green	Greyish brown	Grey	Greyish green
Powder with 1N NaOH	Dark brown	Greenish black	Dark green	Brownish yellow	Blackish green	Dark green	Dark brown	Brownish black	Dark green
Powder treated with Con.H_2SO_4	Brownish black	Black	Green	Yellowish green	Blackish yellow	Dark green	Black	Black	Blackish green
Powder with water	Brown	Brownish black	Light green	Dark green	Dark green	Greenish black	Light green	Grey	Green

Similarly, the powder leaf samples of *Cassia obtusifolia* L. indicated different colour shades like green, brown, and black under the treatment of fluorescence analysis (Kewatkar, 2021). Exposure of *Ficus retusa* L. root and bark powders, *Emblica ribes* leaf powders under various chemical treatments revealed noted fluorescence effects under visible and UV light (Chauhan *et al.,* 2019; Kamble and Gaikwad, 2019).

4.1.2. Qualitative Analysis of Phytochemicals

Phytochemical screening was conducted on leaf, root, and stem extracts of *S. articularis* using methanol, ethanol, acetone, and aqueous solvents. **Table 4.3** displays the results of the qualitative analysis of phytocompounds in *S. articularis.* A broad spectrum of phytochemicals, except for reduced sugars, starch, eugenol, and the anthraquinines, was exhibited in stem methanolic and leaf ethanolic extracts. Tannins, protein, coumarins, fixed oils, and acidic compounds were present in all the extracts, alkaloids, saponins, and oxalates in moderate amounts in all the stem, leaf, and root extracts, while anthocyanins and phytosterols were present in trace amounts. Among the twenty-seven compounds, the leaf and stem extracts of *S. articularis* exhibited a higher presence of phytochemicals compared to root extracts and were therefore selected for further research.

A similar profile of bioactive compounds was observed by Anupriya *et al*. (2016), including alkaloids, coumarins, phenols, quinones, flavonoids, glycosides, saponins, steroids, tannins, and terpenoids in the *Spermococe hispida* methanol extract of the whole plant. Similarly, Rahu *et al*. (2021 found a range of phytochemicals in methanolic extracts of different parts of *Jatropha curcus*, which included phenolics, tannins, saponins, phytosterols, terpenoids, alkaloids, and phlobatannins. A similar array of compounds, such as alkaloids, saponins, flavonoids, glycosides, phenols, tannins, and steroids, in various root extracts of *Rubia cordifolia* was reported by Mishra *et al*. (2021).

Table 4.3. Qualitative analysis of phytochemicals in *S. articularis* leaf, stem, and root extracts

Phyto-constituents	Stem					Leaf				Root		
	SM	SE	SA	SW	LM	LE	LA	LW	RM	RE	RA	RW
Alkaloids	-	+	+	-	-	+	+	-	+	-	++	-
Tannins	++	++	++	+	+	+	+	+	++	+	++	++
Phenols	+	++	++	+	++	+	++	++	+	-	-	-
Saponins	+	-	+	+	+	++	-	+	+	-	-	+
Proteins	++	++	++	+	++	++	++	+	++	++	++	+
Anthocyanin	+	+	-	-	+	+	-	-	-	-	-	-
Quinone	-	++	-	+	+	-	++	++	-	-	-	-
Oxalate	+	+	-	-	+	+	-	-	+	+	++	+
Flavonoids	+	-	+	+	+	+	-	+	+	+	+	+
Vitamin C	++	++	+	+	+	+	+	+	+	+	++	-
Carbohydrates	++	++	++	+	++	++	+	+	-	-	-	+
Phytosterols	-	+	-	-	++	++	+	-	-	-	++	-
Coumarins	+	+	++	+	++	+	+	++	++	++	++	+
Terpenoids	+	+	+	+	+	+	-	+	+	+	+	+
Volatile oil	+	++	+	-	++	++	+	-	+	-	+	-
Resins	+	+	+	+	-	-	+	++	-	+	+	-
Carotenoids	+	+	-	-	+	+	-	-	+	+	++	+
Glycosides	++	+	+	-	++	++	++	-	+	+	++	+
Fixed Oils & Fats	++	++	++	+	+	+	+	++	++	++	++	+
Catechin	++	++	++	++	++	++	++	+	++	++	+	++
Reducing sugar	-	-	-	-	-	-	-	-	-	-	-	-
Amino acids	+	-	-	+	++	-	-	-	+	-	-	+
Starch	-	-	-	-	-	-	-	+	-	-	-	-
Acidic compounds	+	++	++	+	+	++	++	+	++	+	++	+
Eugenol	+	-	-	+	++	-	-	-	+	+	+	-
Cardiac glycosides	++	++	-	+	+	+	-	+	-	-	+	-
Anthraquinone	-	-	-	-	-	-	-	-	-	-	-	-

++ indicates highly present, + indicates presence, - indicates absence
SM: Stem Methanol, SE: Stem Ethanol, SA: Stem Acetone, SW: Stem Aqueous
LM: Leaf Methanol, LE: Leaf Ethanol, LA: Leaf Acetone, LW: Leaf Aqueous
RM: Root Methanol, RE: Root Ethanol, RA: Root Acetone, RW: Root Aqueous

4.1.3 Quantification of Phytochemical Constituents

The estimation of primary metabolites (proteins and carbohydrates) and secondary metabolites (alkaloids, terpenoids, and tannins) in leaf and stem extracts of methanol, ethanol, acetone, and aqueous extracts were studied.

4.1.3.1 Estimation of Primary Metabolites

Primary metabolites play a vital role in the growth and development of plants and also serve as precursors or key components in pharmaceutical compounds. The quantitative analysis revealed that the variation in protein and carbohydrate content was based on the solvents used for extraction, in leaf and stem extracts of *S. articularis*. Methanol extracts exhibited the highest protein content of 27.65 ±0.009 mg/g in stem and 15.64±0.005 mg/g in leaf. Aqueous and acetone extracts recorded the lowest protein content of 10.12±0.08mg/g and 12.53±0.002mg/g in leaves. Methanol extracts showed the highest carbohydrate content (184.44±0.005 mg/g in the stem and 152.4±0.032 mg/g in the leaf) in the methanol extracts, while the lowest carbohydrate content (10.72±0.018 g/100g in leaves and 19.32±0.010 g/100g in stem) was observed in the aqueous extracts (Table 4.4).

Table 4.4 Quantification of primary metabolites in *S. articularis* leaf and stem extracts

Samples	Solvent	Protein (mg/100g)	Carbohydrates (mg/100 g)
Leaf	Acetone	12.53±0.002	144.01±0.057
	Methanol	15.64±0.005	152.4±0.032
	Ethanol	14.19±0.010	136.2±0.021
	Aqueous	10.12±0.08	10.72±0.018
Stem	Acetone	20.52±0.006	172.52±0.009
	Methanol	27.65±0.009	184.44±0.005
	Ethanol	22.95±0.018	177.43±0.012
	Aqueous	19.17±0.013	19.32±0.010
SED		0.28±0.005	1.05±0.005
CD (0.05)		0.64±0.005	0.47±0.005

Values represent the mean±SD of three replicates

High protein content in the plant indicated its potential nutritional value and opportunities for discovering novel bioactive compounds (Talreja, 2011). A recent study by Sarkar *et al*. (2020) reported that *Psidium guajava* exhibited the highest protein content, with 98.51 mg/g of fresh weight, followed by red *Amaranthus viridis* (97.43 mg BSAE/g of FW) and *Justicia adathoda* (86.37 mg BSAE/ g of FW). Banik *et al.* (2019) reported protein and carbohydrate content variations in *Centella asiatica* (4.98%v/v and 97.67%w/v), followed by *Ficus bengalensis* (6.38%v/v and 78.02%w/v) and *Stellaria media* (10.05%v/v and 75.27% w/v), respectively and the *Cinnamomum tamala* demonstrated the highest protein content of 10.64% v/v, and the lowest carbohydrate content of 19.71% w/v.

4.1.3.2 Estimation of Secondary Metabolites

The quantitative analysis of major phytochemicals such as alkaloids, terpenoids, and tannins was conducted using standard procedures. The quantification of secondary metabolites estimated in methanol, ethanol, acetone, and aqueous extracts of the leaf and stem of *S. articularis* is graphically represented in **Figure 4.1.**

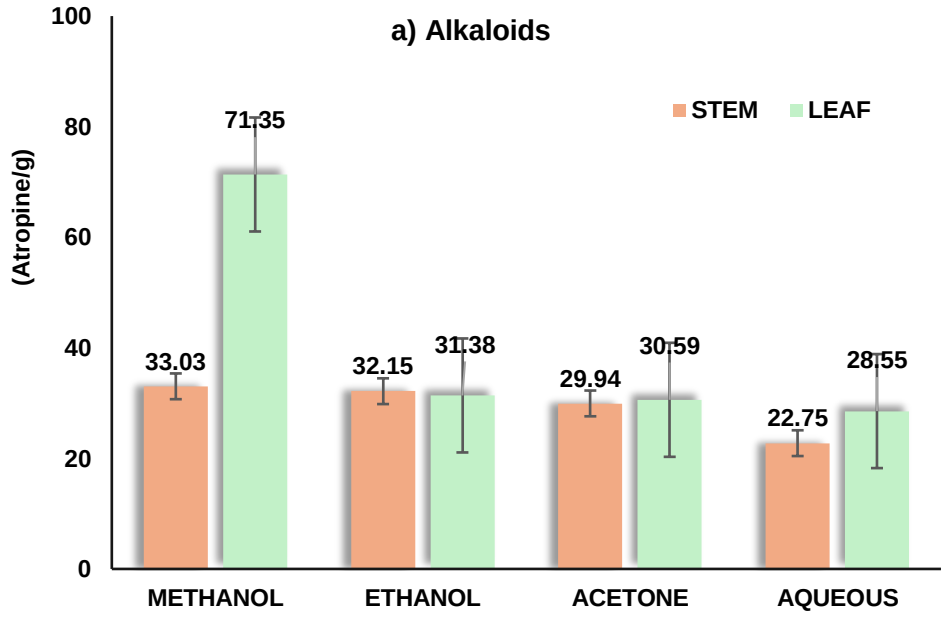

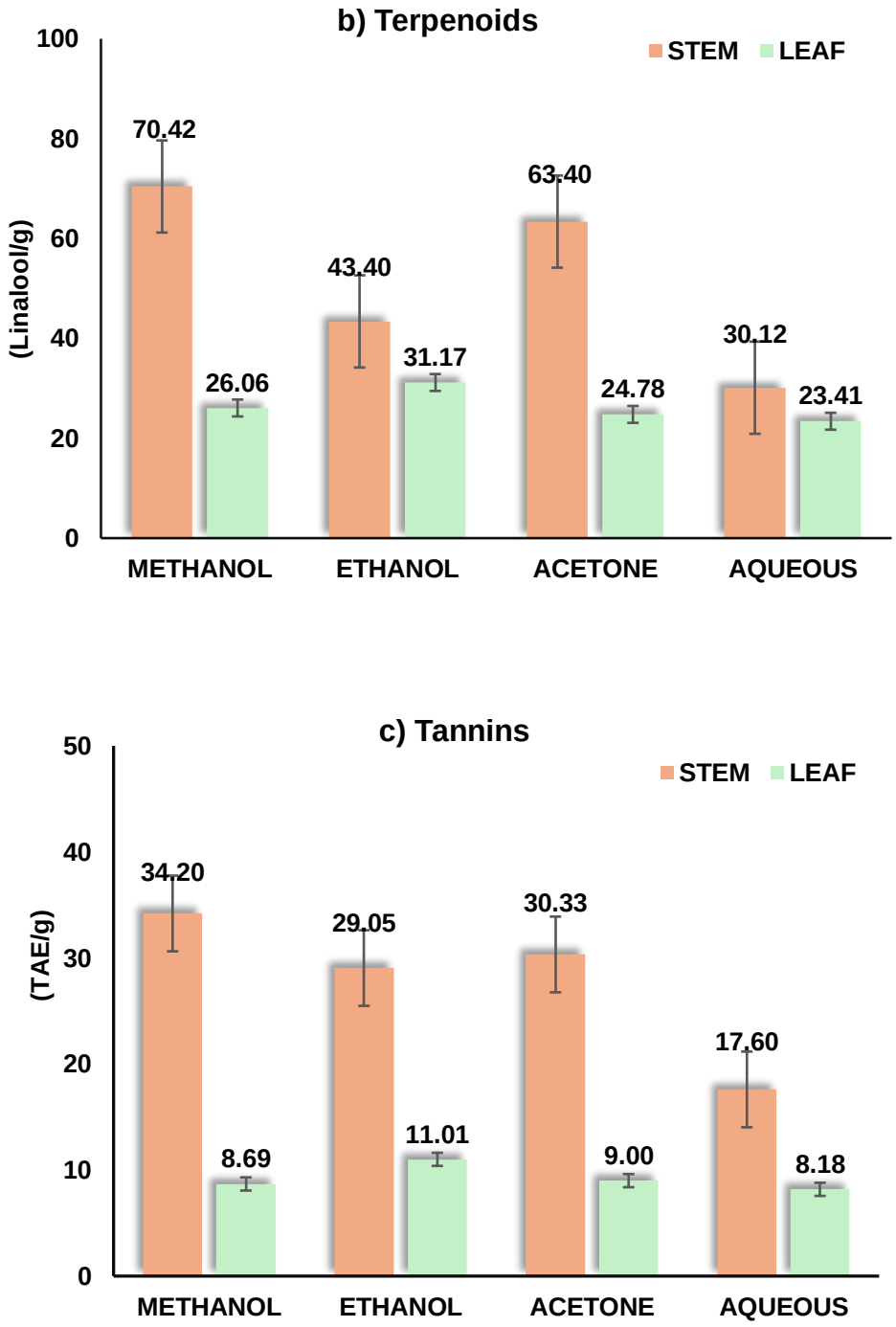

Figure 4.1. Quantification of secondary metabolites in the different extracts of *S. articularis* Leaf and Stem
a) Alkaloids, b) Terpenoids, and c) Tannins

The methanol extracts of the stem and leaf exhibited the highest content of alkaloid (71.35±0.0049 mg atropine/g), terpenoids (70.42±0.001 mg linalool/g), and tannins (34.20±0.005 mg TAE/g), and the minimum content was observed in aqueous extracts of the leaf (28.55±0.0051 mg atropine/g, 8.18±0.001 mg linalool/g, 23.41±0.001 mg TAE/g) and stem (22.75±0.001 mg atropine/g, 17.60±0.014 mg linalool/g, 30.12±0.001 mg TAE/g). Anupriya *et al*. (2016) reported a tannin content of 11.04 mg/g and an alkaloid content of 10.42 mg/g in the methanol extract of *Spermacoce hispida* whole plant. Similarly, Chopade *et al*. (2023) and Towanou *et al*. (2023) found significant amounts of tannins in ethanol leaf extracts of *Ardissi asolanacea* (148.23±0.510 mg TAE/g) and *S. italica* (2.74±0.15 mg CE/g).

4.1.4 Evaluation of Antioxidant Activity

The evaluation of enzymatic and non-enzymatic antioxidants was focused on the leaf and stem extracts using methanol, ethanol, acetone, and aqueous solvents, and the results are discussed below.

4.1.4.1 Estimation of Enzymatic Antioxidants

The increasing demand for natural antioxidants as substitutes for synthetic ones has driven research into plant-based sources, leading to the discovery of new antioxidants through the screening of raw materials. The preliminary phytochemical analysis of *S. articularis* revealed that the stem and leaf extracts contain more active components compared to root extracts. The maximum content of enzymatic antioxidants, such as polyphenol oxidase (2.88 units/g), peroxidase (1.688 units/g), ascorbate oxidase (0.759 units/g), and catalase (0.758 units/g), was observed in the methanol stem extract, followed by the ethanol stem extract. The leaf showed maximum content of enzymatic antioxidants of polyphenol oxidase (1.885 units/g), peroxidase (1.247 units/g), catalase (0.702 units/g), and ascorbate oxidase (0.496 units/g) in ethanol extract when compared to other solvent extracts. Enzymatic antioxidants were maximum in the stem sample compared to the leaf sample, exhibiting various antioxidant activities to support their utility **(Figure 4.2).**

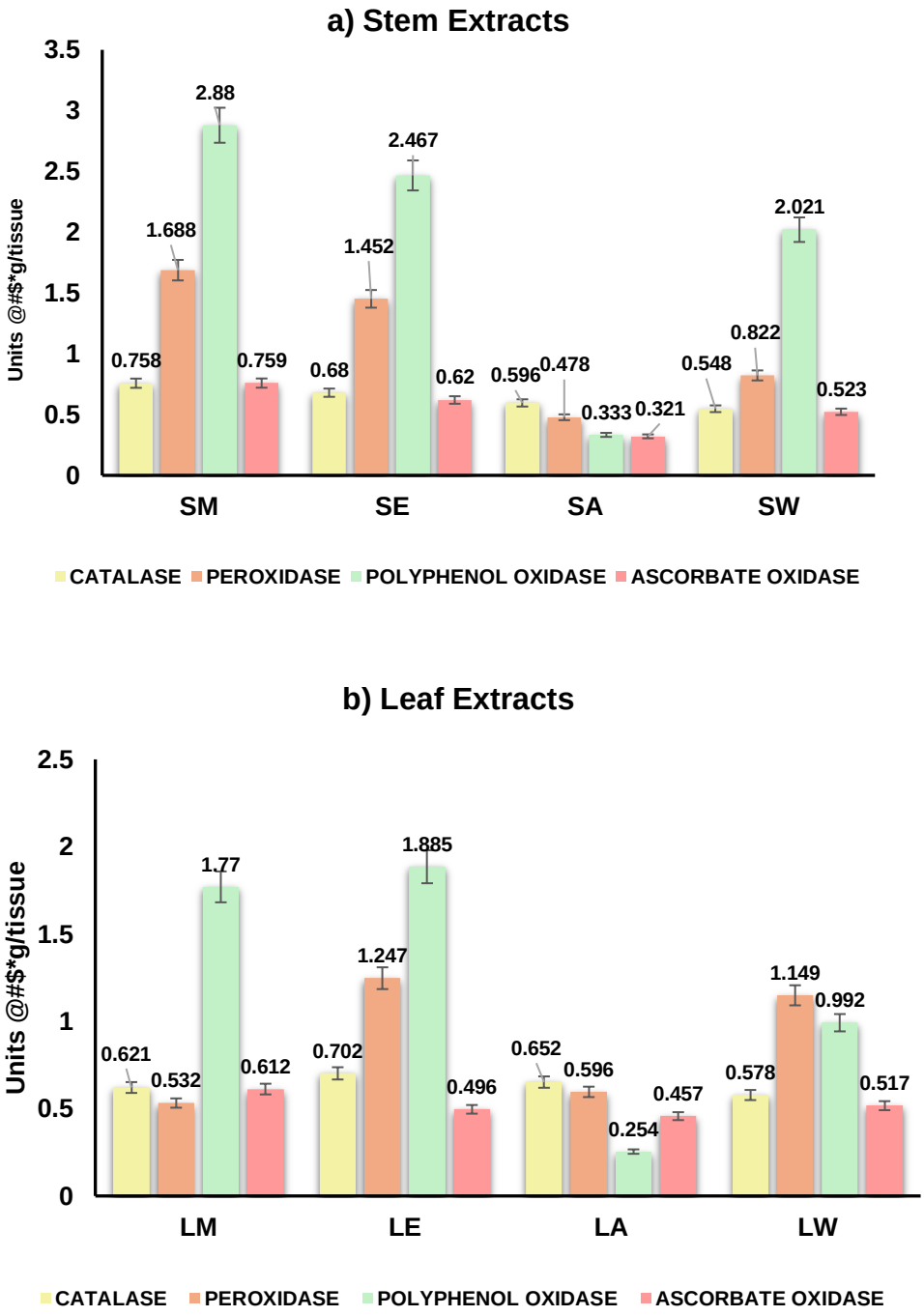

Figure 4.2 Estimation of enzymatic antioxidants of *S. articularis*

a) Stem Extracts b) Leaf Extracts

SM: Stem Methanol, SE: Stem Ethanol, SA: Stem Acetone, SW: Stem Aqueous; LM: Leaf Methanol, LE: Leaf Ethanol, LA: Leaf Acetone, LW: Leaf Aqueous. @- One unit is defined as the amount of enzyme required to decrease the OD by 0.05 units at 240nm; #- One unit is defined as the changes in absorbance at 430nm/ minute; $- Changes in absorbance at 495nm/minute; *-One unit is equal to 0.01 OD changes per minute.

The phytochemical results of the present study coincide with those of Vijayakumari *et al.* (2016), who reported high peroxidase activity in the fruit extract of *Emblica officinalis*. Muthu and Durairaj (2015) reported that the hydroalcoholic extract of *Annona muricata* leaves contained the highest level of polyphenol oxidase. Krishna *et al.* (2012) observed significant ascorbate oxidase activity in *Amorphophallus commutatus*, with the highest activity in the tuber (0.38 Units/g tissue), followed by young leaves (0.010 Units/g tissue) and mature leaves (0.005 Units/g tissue).

4.1.4.2 Evaluation of Non-Enzymatic Antioxidants

The compounds that inhibit free radicals and defend cells against oxidative damage without enzymatic activity are the non-enzymatic antioxidants. In addition to enzymatic antioxidants studied, non-enzymatic antioxidants, such as total phenolic content, total flavonoid content, ascorbic acid (vitamin C), and alpha-tocopherol (vitamin E) were also estimated.

4.1.4.2.1 Estimation of Total Phenolic Content

Phenolic compounds in plants are potent antioxidants that effectively scavenge free radicals, acting as reducing agents and hydrogen donors, thereby indicating the plant's antioxidant potential (Wojdylo *et al.,* 2007). The total phenolic content of the leaf and stem extracts of *S. articularis* was estimated, followed by the method of Folin-Ciocalteau, compared with the standard gallic acid. The total phenolic content was calculated based on the obtained calibration curve of gallic acid ($y=0.0821x-0.001$; $R^2=0.993$) using the absorbance values at different concentrations ranging from 0.2-1.0 mg/ml. At 10mg/ml of concentration, the stem acetone extract of *S. articularis* exhibited maximum phenolic content (15.26±0.003 mg/ml) than the leaf ethanol extract (23.64±0.004 mg/ml). In contrast, stem ethanol extract and aqueous leaf extracts expressed a minimum phenolic content of 8.89±0.001 mg/ml and 8.2±0.001 mg/ml, respectively (**Figure 4.3**).

The total phenolic content of *S. hispida* is found to be 6.88 mg CAE and 9.17 mg TAE, highlighting a significant correlation between phenolic content and antioxidant potential (Ankad *et al.* 2015). Our results are in line with Priyadarshini *et al.* (2017), who reported higher phenolic compounds in leaf extracts compared

to stem extracts. Prabhu *et al.* (2016) found a significant correlation between total phenolic content and antioxidant activity in *S. hispida* leaves, highlighting its contribution to medicinal properties. The methanol extracts of *Acacia hockii* had the highest total phenolic content of 41.78 mg GAE/g compared to *Vernonia lasiopus* of 6.04 mg GAE/g and *Caesalpinia volkensii* of 28.51 mg GAE/g (Guchu *et al.,* 2020). A significant total phenolic content in *Bergenia ciliate* (27.48 mg GAE/g), *Aloe vera* (25.61 mg GAE/g), and *Achillea millefolium* (24.25 mg GAE/g) methanol extracts were observed by Mehmood *et al.* (2022).

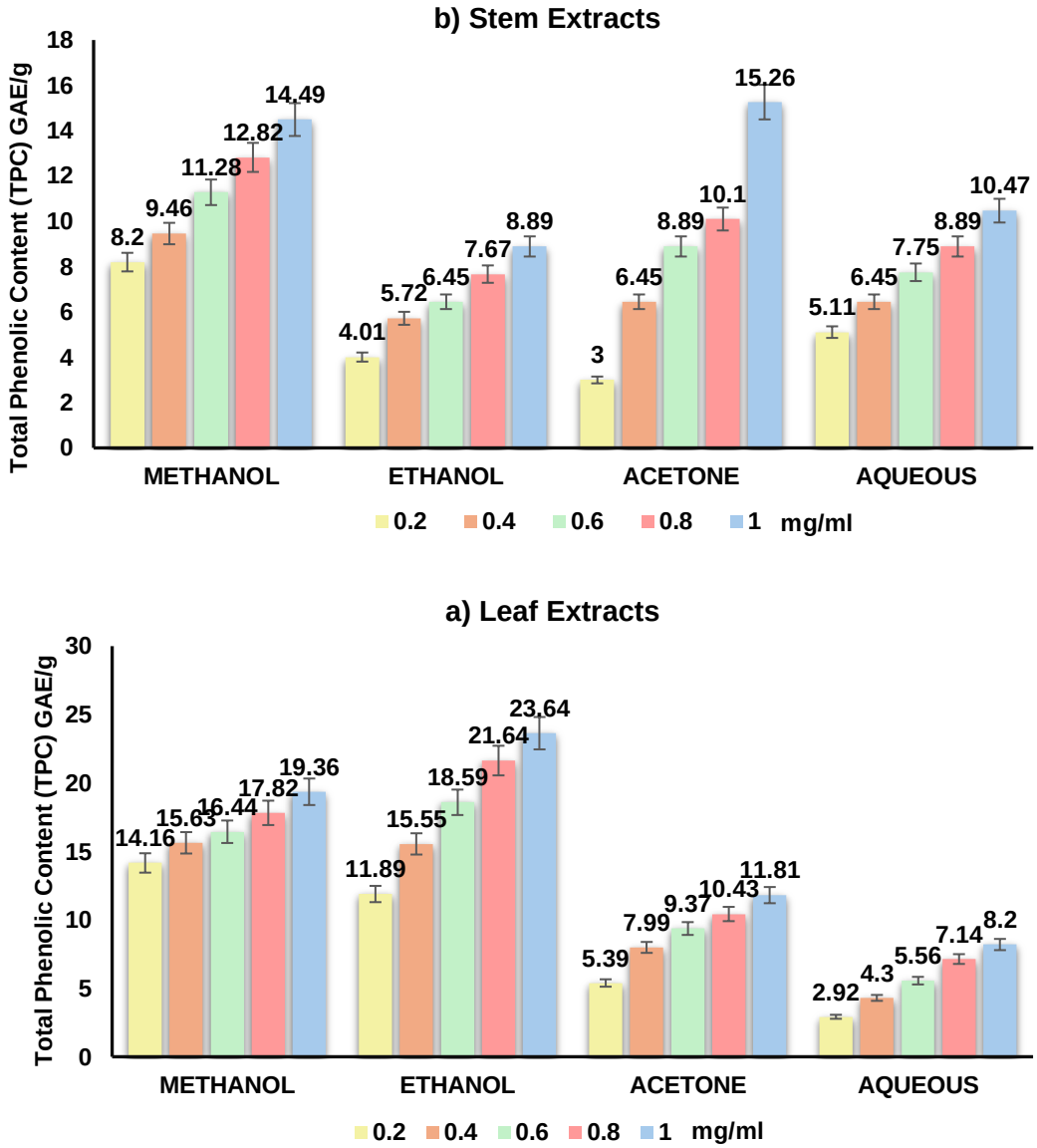

Figure 4.3. Estimation of total phenolic content of *S. articularis*

a) Stem Extracts b) Leaf Extracts

4.1.4.2.2 Estimation of Total Flavonoid Content

The total flavonoid content of different *S. articularis* extracts is shown in Figure **4.4.** The total flavonoid content was calculated using rutin as a standard at concentrations ranging from 0.2 to 1.0mg/ml. The calibration curve showed a linear relationship with y=0.057 + 0.0086 with a strong correlation (R^2=0.9915). Among all other extracts, the methanol extracts of stems and leaves exhibited the highest flavonoid content, with values of 385.49 ± 0.006 mg/ml and 118.24±0.003 mg/ml, respectively.

TFC values have been reported for various plant extracts, including *Spermacoce italica* (898.36±4.04 mg QE/g) by Towanou *et al*. (2023), *Citrus acida* (181.47±3.65 mg QEE/g) by Jain *et al.* (2021), *Bathys agymnocarpa* (70.07±1.5 mg RE/g) by Araujo *et al*. (2023), and *Ardissia solanacea* (371.91±0.167 mg QE/g) by Chopade *et al.* (2023), consistent with our present study.

4.1.4.3 Estimation of Ascorbic Acid and α-Tocopherol

All the solvent extracts of *S. articularis* stem and leaf exhibited higher levels of ascorbic acid compared to α-tocopherol (**Figure 4.5**). Among the stem extracts, the highest ascorbic acid (3.023±0.002 units/g) and α-tocopherol (0.853±0.004 units/g) were found in methanol. In the leaf, significant levels of ascorbic acid (2.986±0.006 units/g) and α-tocopherol (0.713±0.012 units/g) were found in ethanol extracts compared to other extracts.

In a similar study, Iniyavan *et al.* (2012) found the highest ascorbic acid content in *Psychotria nilgiriensis* fruit extract, while Varalakshmi *et al.* (2012) observed in *Cinnamomum zeylanicum* bark extract. Additionally, Srinivasan and Durairaj (2014) reported α-tocopherol content of 83.5±0.5 µg/g in *Morinda citrifolia* fruit.

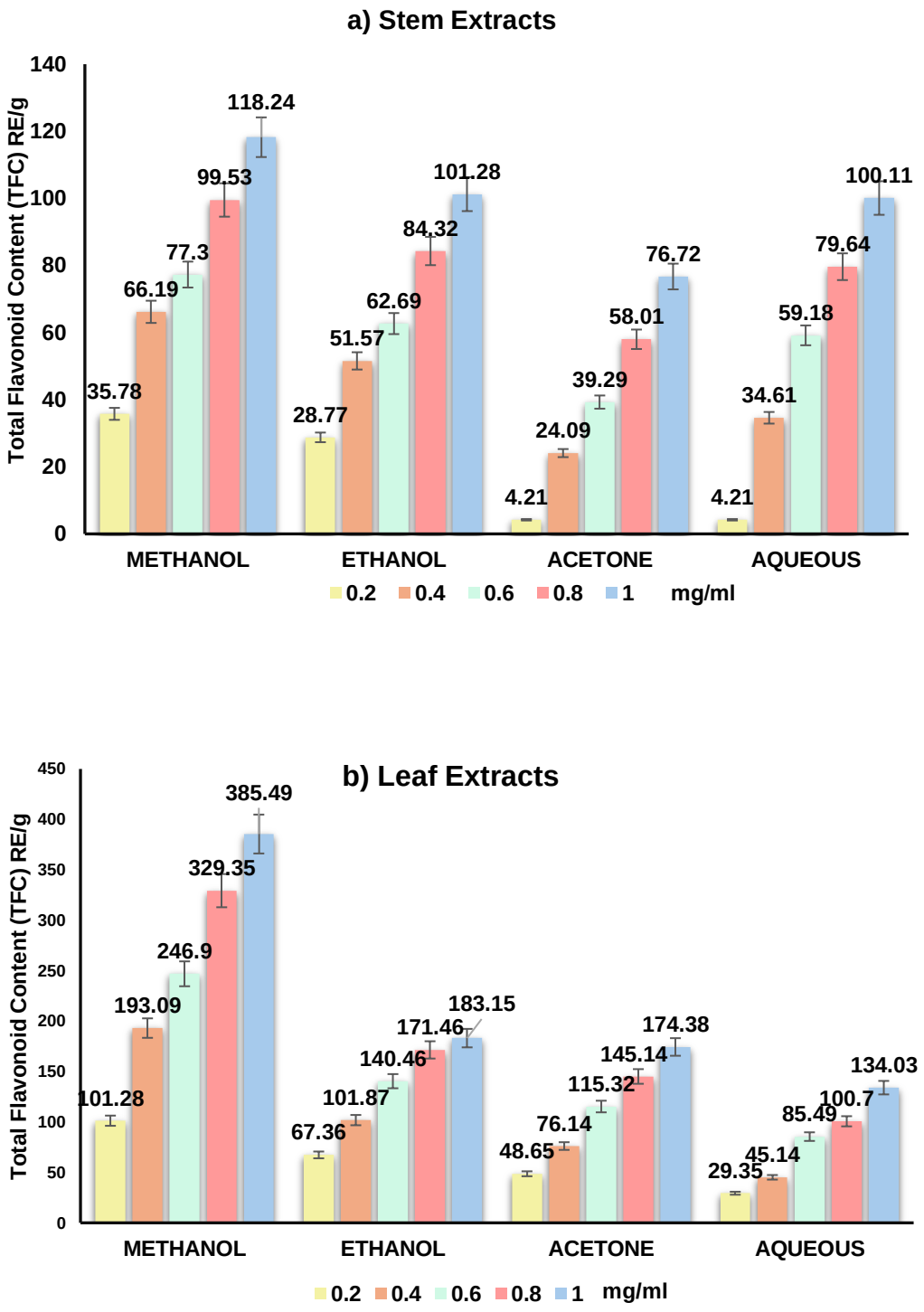

Figure 4.4. Estimation of total flavonoid content of *S. articularis*
a) Stem Extracts b) Leaf Extracts

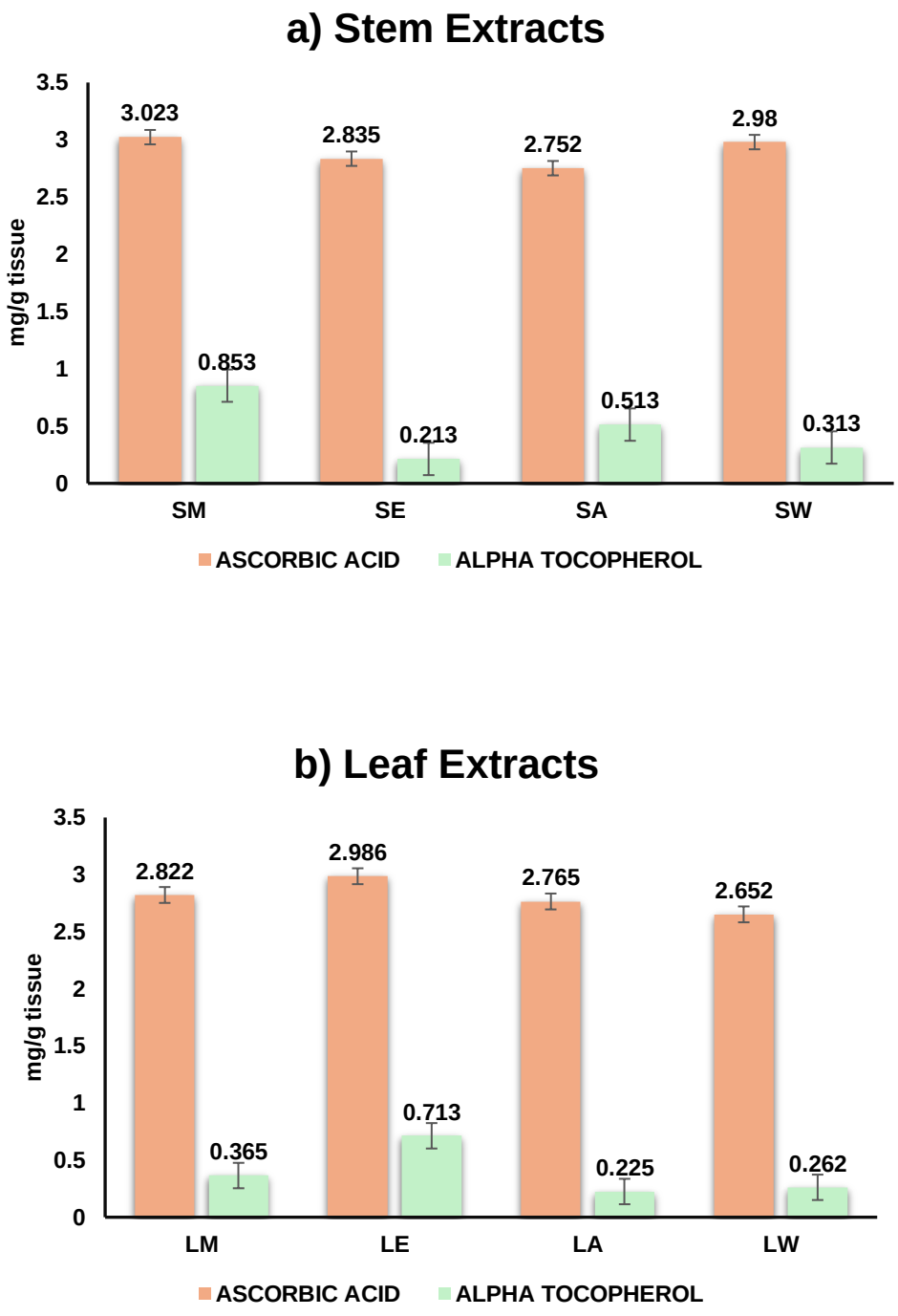

Figure 4.5. Estimation of ascorbic acid and α-tocopherol of *S. articularis* a) Stem Extracts b) Leaf Extracts

SM: Stem Methanol, SE: Stem Ethanol, SA: Stem Acetone, SW: Stem Aqueous

LM: Leaf Methanol, LE: Leaf Ethanol, LA: Leaf Acetone, LW: Leaf Aqueous

4.1.5 *In vitro* Radical Scavenging Assay

In vitro radical scavenging activity assesses the antioxidant activity of various compounds or extracts by evaluating the ability of antioxidants to counteract free radicals, which are reactive and unstable molecules responsible for oxidative stress and damage to cells. This is done through assays such as DPPH, ABTS, and FRAP, offering valuable insights into their potential benefits in preventing or treating oxidative stress-related diseases.

The phytochemical and antioxidant studies showed that the stem methanol and leaf ethanol extracts exhibited the highest activities. Hence, based on these results, these two extracts were chosen for further free radical scavenging assays to assess their antioxidant potential.

4.1.5.1 DPPH Radical Scavenging Assay

In the DPPH assay, the antioxidants reduced the stable radical DPPH from purple to yellow colour. The results demonstrated a dose-dependent reduction in DPPH activity by the extracts and standard, ascorbic acid **Figure 4.6.**

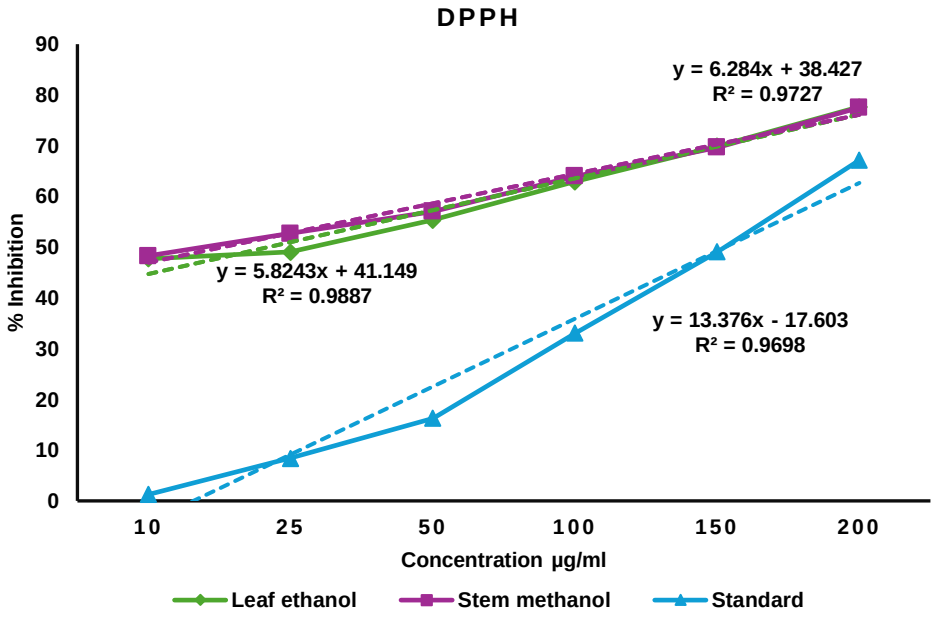

Figure 4.6 DPPH radical scavenging potential of *S. articularis* leaf and stem extracts

DPPH radical scavenging potential was also evaluated based on IC_{50} values, representing the required concentration of an antioxidant to neutralize 50% of the initial DPPH radicals. A lower IC_{50} value indicated higher antioxidant activity. *S. articularis* exhibited the IC_{50} value of 49.5±0.342% µg AA/ml for stem methanol extracts and 23.55±1.270% µg AA/ml for leaf ethanol extract, whereas the standard (Ascorbic acid) showed an IC_{50} value of 53.05±1.67% µg/ml, indicating that *S. articularis* leaf and stem extracts possessed powerful antioxidant potential.

Spermacoce latifolia whole plant extracts showed IC_{50} values ranging from 22.52 to 72.12 µgAA/ml, with the aqueous extract exhibiting the highest activity (Luo *et al.,* 2020). *Citrus acida* ethanol extract showed an IC_{50} value of 40.44 µg AA/ml (Jain *et* al., 2021), while *Rubia cordifolia* methanol root extract had 78.1 µg AA/ml (Mishra *et al.,* 2021). *Coffea benghalensis* stem ethyl acetate extract showed significant antioxidant activity with an IC_{50} value of 3.22% µg BHT/ml (Sagor *et al.,* 2021), and *Bergenia ciliata* methanol extract exhibited an IC_{50} of 60.27 µg/ml (Mehamood *et al.,* 2022).

4.1.5.2 Ferric Reducing Antioxidant Power Assay

The Ferric Ion Reducing Antioxidant Power (FRAP) assay is an electron transfer-based method where the ferricyanide complex is reduced to its ferrous from (Fe2+), causing a colour change from yellow to green or blue, indicating the sample's reducing power (Huda-Faujan *et al.,* 2009).

Results showed that *Spermacoce articularis* stem and leaf extracts exhibited significant reducing power, increasing with concentration (10-200 µg/ml). The standard gallic acid showed higher activity with an FRAP value of 54.02±0.101 µg/ml (**Figure 4.7**). However, the stem methanol and leaf ethanol extract demonstrated lower values of 13.84±0.085 µg GAE/ml and 37.5±0.0026 µg GAE/ml, respectively, indicating higher activity compared to the standard.

Sagor *et al.* (2021) found that *Coffea benghalensis* stem ethyl acetate extract exhibited its strongest reducing power at 400 µg/ml, achieving 1.455±0.08% inhibition. In another study, Mishra *et al.* (2021) reported IC_{50} values of 1.52 µM for *Rubia cordifolia* methanol root extract at a concentration of 500 µg/ml. Furthermore, Zengin *et al.* (2023) observed IC_{50} values of 664.85 mg TE and 996.70 mg TE for *Paliurus spina*-christi leaf and stem methanol extracts, respectively.

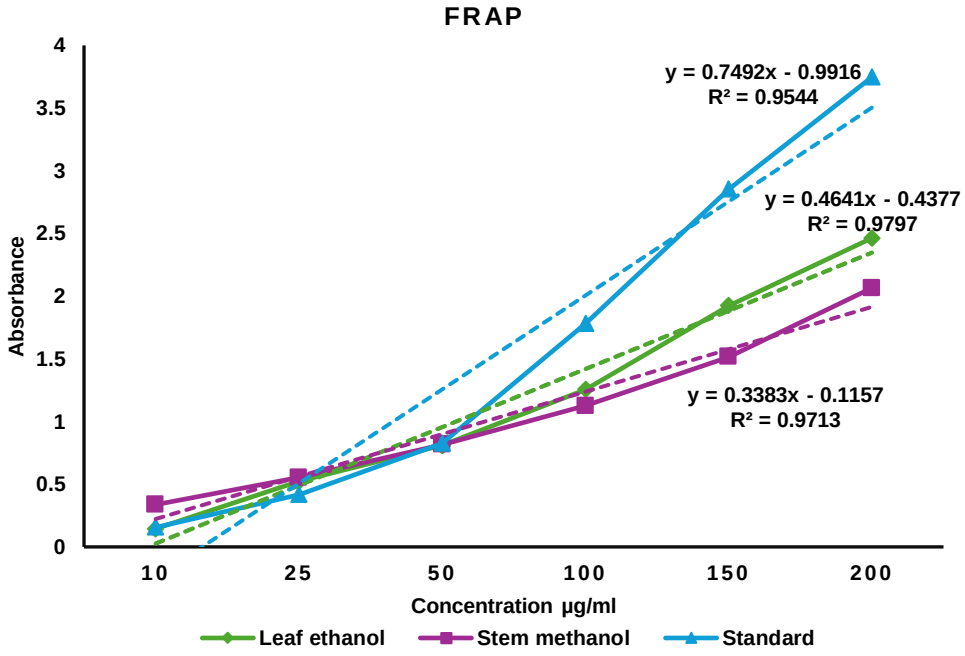

Figure 4.7 Ferric reducing power of *S. articularis* leaf and stem extracts

4.1.5.3 ABTS Radical Scavenging Assay

The ABTS+ assay evaluates the antioxidant activity through electron transfer, where the antioxidants reduce a dark blue ABTS+ radical cation into colourless ABTS, which can be measured spectrophotometrically. The ABTS+ radical scavenging potential of plant extracts and standards increased with concentration (10-200 µg/ml) (**Figure 4.8**).

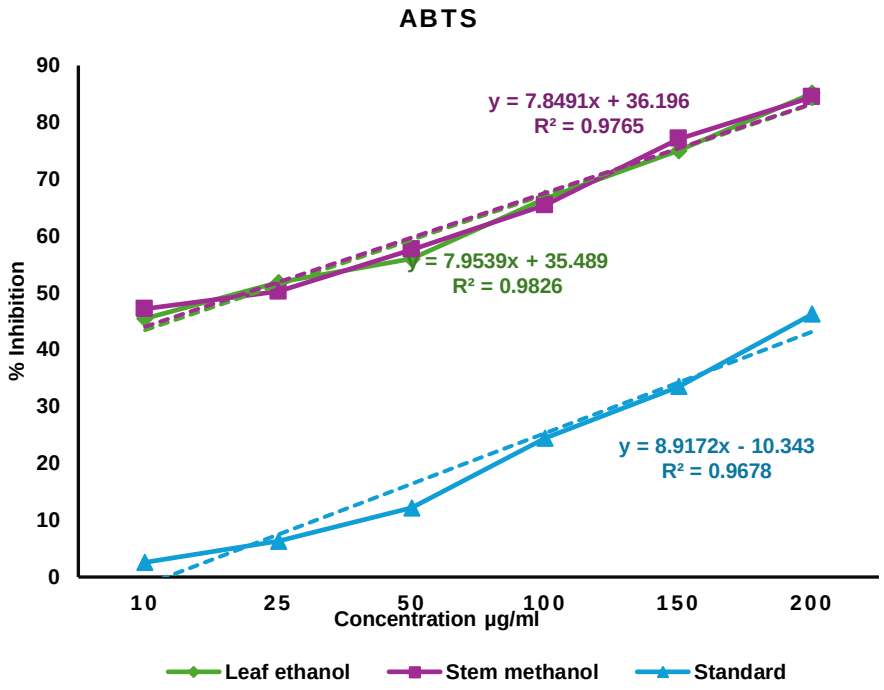

Figure 4.8 ABTS radical scavenging potential of *S. articularis* leaf and stem extracts

The plant extracts demonstrated potent scavenging activity, with significantly lower IC_{50} values compared to the standard gallic acid (46.94±0.494 µg/ml). Specifically, the stem methanol extract and ethanol leaf extract exhibited IC_{50} values of 20.08±0.144 µg GAE/ml and 22.48±0.637 µg GAE/ml, respectively, indicating strong antioxidant potential. The results confirmed the presence of antioxidants, as evidenced by a linear decrease in absorption and a corresponding decolorization that was positively correlated to the increasing antioxidant capacity of the extract.

According to Mistral *et al*. (2024), vitamin C had stronger antioxidant activity than the hydro-ethanolic extract of *Spermacoce ocymoides* in the ABTS assay, as indicated by IC_{50} values of 13.09±1.87 µg/mL and 43.01±12.39 µg/mL, respectively. (P=0.01). Adebiyi *et al.* (2017) reported an IC_{50} value of 58.15% and 70.25% mg AA /ml for the leaves and stems of *Grewia carpinifolia*, respectively. The results are in accordance with Luo *et al.* (2020), who reported the IC_{50} values of various fractions of petroleum ether (14.36±0.13 µgAA/ml), ethyl acetate

fraction (10.94±0.11 µgAA/ml), n-butanol (15.40±0.09 µgAA/ml), and aqueous (162.22±1.39 µgAA/ml), respectively, in the whole plant crude extracts of *S. latifolia.* The IC_{50} value of ethanol extract was found to be 58.46 µg/ml in *Citrus acida* leaf (Jain *et al.,* 2021) and 1171.58 mg TE in *Paliurus spina-christi* Leaf (Zengin *et al.,* 2023).

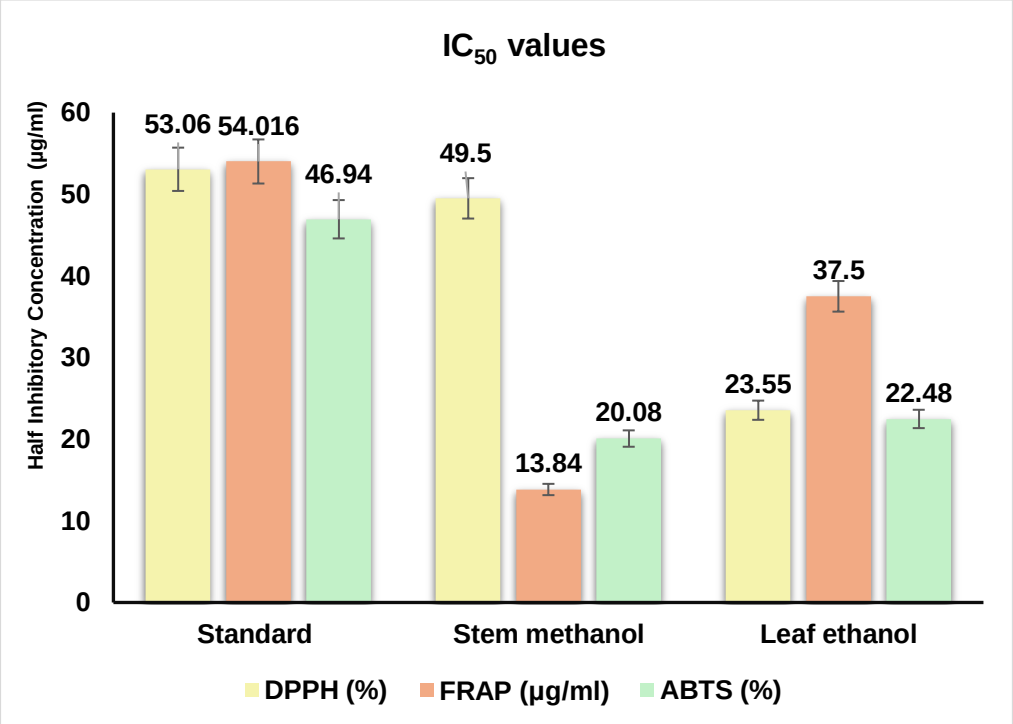

Figure 4.9 The free radical scavenging potential of *S. articularis* leaf and stem extracts

Phase I of the study evaluated the phytochemical screening and antioxidant activities of *Spermacoce articularis* extracts. The organoleptic study revealed distinct characteristics among leaf, stem, and root samples. Phytochemical analysis indicated the presence of various compounds, with leaf and stem extracts showing a higher presence of phytochemicals compared to root extracts. Quantitative analysis revealed significant levels of primary metabolites (proteins and carbohydrates) and secondary metabolites (alkaloids, terpenoids, and tannins) in ethanol leaf and methanol stem extracts. Enzymatic antioxidant and non-enzymatic antioxidant activities also showed the highest activities in leaf and stem extracts compared to other extracts. Hence, the

stem methanol and leaf ethanol extracts were further evaluated for free radical scavenging potential using DPPH, FRAP, and ABTS assays, and the results exhibited *S. articularis* as the powerful antioxidant potential. Overall, the study of phase I highlighted the promising phytochemical profile and antioxidant potential of *S. articularis*, particularly in the stem methanol and leaf ethanol extracts.

PHASE II

4.2 Antiurolithiatic Activity of *Spermacoce articularis*

4.2.1 *In vitro* Antiurolithiatic Activity

This study investigated the antiurolithiatic potential of *S. articularis* extracts, evaluating their ability to inhibit calcium oxalate crystal formation, nucleation, and aggregation, providing insights into their therapeutic potential for managing kidney stones. The *in vitro* antiurolithiatic activity of *S. articularis* extracts was evaluated using methanol stem extract (SASM) and ethanol leaf extract at concentrations of 100-600 µg/ml.

4.2.1.1. Effect of *S. articularis* Leaf Ethanol on Calcium Oxalate Crystal Nucleation

Kidney stones formation involves supersaturation, crystallization, growth, and aggregation, and eventual adhesion to the renal epithelium. A key factor in the development of renal calculi is the imbalance between promoters such as albumin, oxalate, and uric acid and inhibitors like citrate, magnesium, nephrocalcin, and urinary prothrombin fragment (Gupta *et al.,* 2011). Inhibition of calcium oxalate crystal nucleation by *S. articularis* ethanol leaf extract at various concentrations is presented in **Figure 4.10a**.

The data represented that the percentage inhibition of CaOx crystal formation after 30 minutes of incubation is directly proportional to the increase in the concentration of the plant extract. At 100 µg/ml concentration of *S. articularis* ethanol leaf extract exhibited a minimum inhibition of 14.77±0.001%, which progressively increased, ultimately reaching a maximum inhibition of 18.2±0.001% at 600 µg/ml. In comparison, cystone demonstrated the highest inhibitory activity, with an inhibition of 65.22±0.003% at 600 µg/ml. The percentage inhibition of *S. articularis* ethanol leaf extract was compared with both the control and cystone. A reduction in solution turbidity caused by the plant extract indicated that the extract was effective in reducing the formation of oxalate crystals, thereby exhibiting a lower level of crystallization compared to the control.

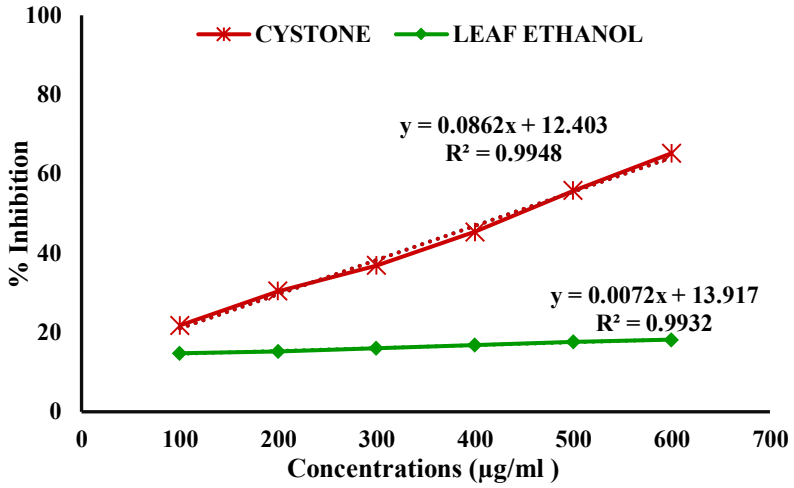

Figure 4.10a. Effect of *S. articularis* leaf ethanol extract on CaOx crystal nucleation

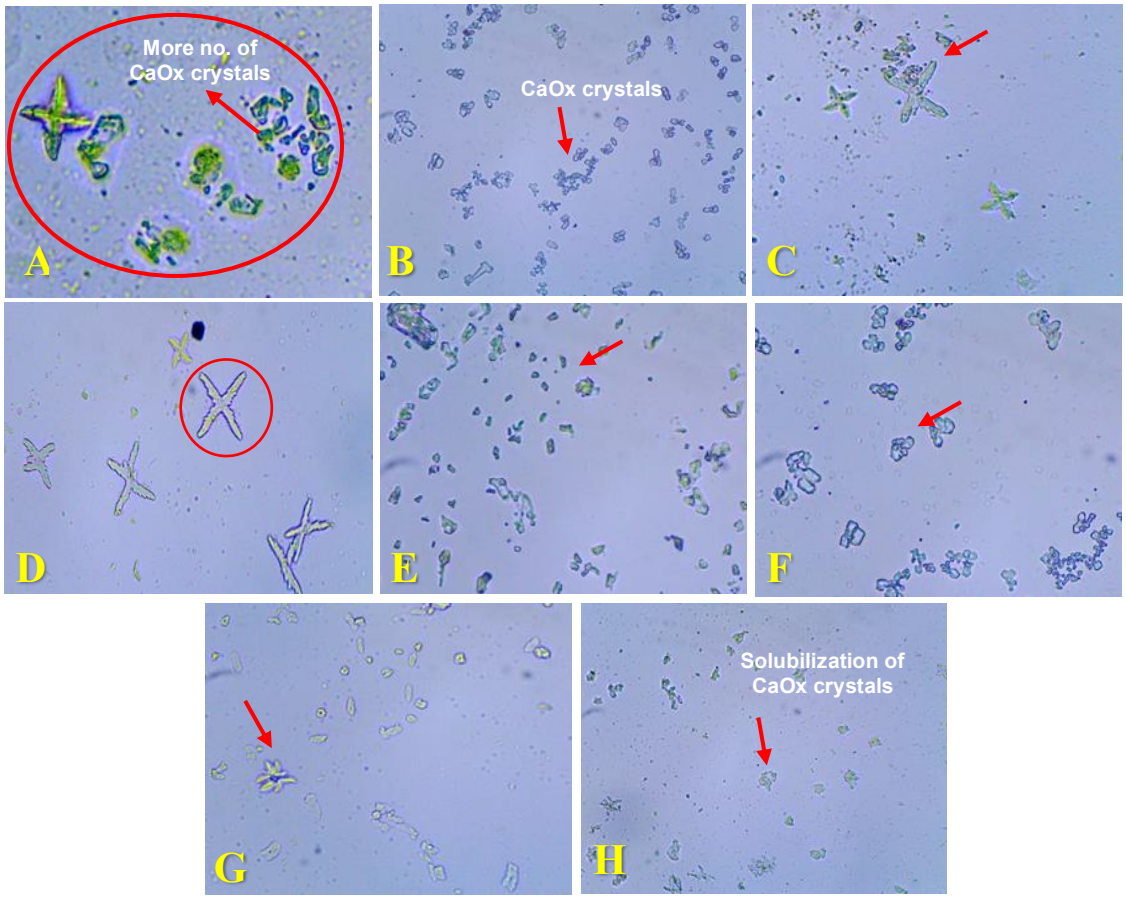

Figure 4.10b. Micrographs of CaOx crystals nucleation in the absence and presence of *S. articularis* leaf ethanol extract at 1000x.

A) Control, B) Cystone, C) 100 µg/ml, D) 200 µg/ml, E) 300 µg/ml, F) 400 µg/ml, G) 500 µg/ml, and H) 600 µg/ml of concentrations

From **Figure 4.10b**, it is observed that in the light microscopic images of A (control), where the ethanol leaf extract and standard were not added, the maximum number of crystals was observed. In contrast, images C–H, representing the plant extract at concentrations ranging from 100–600 µg/ml, showed a reduction in crystal formation, though less pronounced than in image B with cystone at 600 µg/ml. The crystal growth experiment, further confirmed that the ethanol leaf extract produced smaller and fewer crystals, there by slowing the rate of crystal growth compared to the control.

These findings are similar to the results reported by Hewagama and Hewawasam (2022) who reported that the whole plant hexane extract of *Aegle marmelos* exhibited a maximum percentage inhibition of 83.56±0.06%, at a concentration of 1000µg/ml, while the ethanol extract of *Aegle marmelos* at the same concentration showed a significant percentage inhibition of 82.74 ± 0.68%. According to Bawari *et al*. (2018), the *Daucus carota* ethanol root extract at a concentration of 1000 µg/ml demonstrated a significant reduction in nucleation, with a percent decrease of 56.1±1.55% in the reaction mixture. Notably, this inhibitory effect was substantially higher than that exhibited by cystone, which showed a percentage decrease of 41.67±1.03%.

Antiurolithiasis activity of *Sterculia urens* ethanol leaf extract at 600µg/ml showed a significant inhibition of 35% and 27%, respectively, indicating the extract's potential to reduce CaOx crystals than the standard cystone (27%) (Swarnalatha, 2022). Similar to our results, Vishnu Priya and Tamilselvi (2022), observed the leaf ethanol extracts of the *Aerva lanata* and cystone at 500µg/ml exhibited 87.93% and 90% of equivalent inhibitory activity. Solomon *et al.* (2019) reported a 55.73% inhibition at a 30 mg/ml concentration of *Maerua angolensis* leaf ethanol extract.

4.2.1.2. Effect of *S. articularis* Stem Methanol (SASM) Extract on Calcium Oxalate Crystal Nucleation

Using a spectrophotometric assay, the inhibitory effect of the extraction on the CaOx crystals nucleation was assessed (Saha and Verma, 2015). The addition of the SASM extract to the solution indicated fragmentation of oxalate crystals after an incubation period of 30 minutes. The plant extract inhibited CaOx crystals in a dose-dependent manner, expressing greater inhibitory effects. All concentrations of the SASM extract exhibited a significant reduction in the nucleation of CaOx crystals compared to the standard.

The stem methanol extract of *S. articularis* showed the highest inhibition rate of 67.16±0.002%, comparable to cystone 65.22 ± 0.003% at 600µg/ml of concentration (**Figure 4.11a**). Light microscopy revealed a high number of crystals in the control group (**Figure 4.11b-**A). In contrast, the plant extract exhibited a maximum inhibition effect at concentrations between 100-600 µg/ml, similar to cystone at 600 µg/ml (B-H). Crystal formation occurred in a dose-dependent manner after 30 minutes of incubation. The crystal growth experiment evaluated the rate of growth at different concentrations, with and without stem methanol extract, over a constant time.

Nucleation is the spontaneous crystallization of dissolved substances in a supersaturated solution, driven by a thermodynamic phase change. The extract demonstrated a significant inhibition of CaOx crystal nucleation when compared to cystone. Furthermore, the extract reduced the size of the crystals formed, demonstrating its growth inhibitory capabilities. This indicated that the extract exhibits anti-crystallization activity in the CaOx crystallization assay. The extract may have anti-crystallization properties by forming free calcium and oxalate ion complexes, thereby inhibiting the formation of CaOx crystals. Reducing the size of CaOx crystals enhances their spontaneous dissolution in urine, thereby preventing their growth and potential formation of kidney stones (Agarwal and Varma, 2015; Sheng *et al*., 2005).

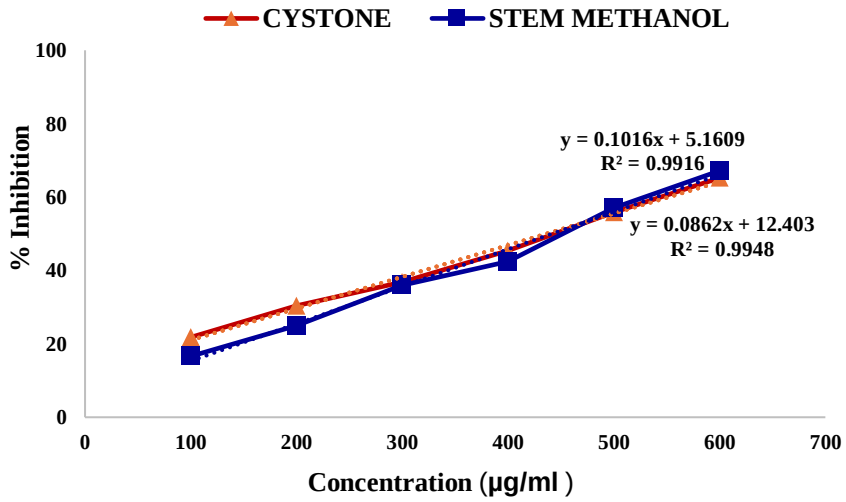

Figure 4.11a. Effect of SASM extract on CaOx crystal nucleation.

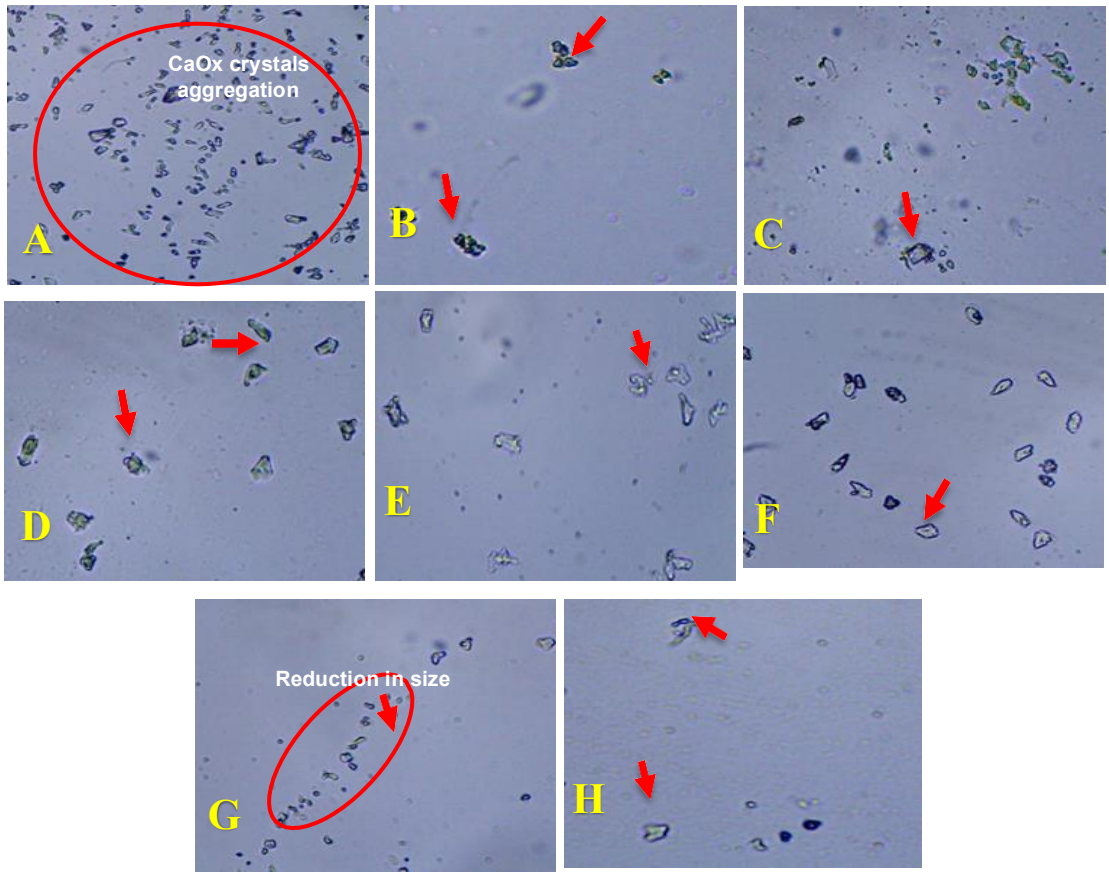

Figure 4.11b. Micrographs of CaOx crystals nucleation in the absence and presence of SASM extract.

A) Control, B) Cystone, C) 100 µg/ml, D) 200 µg/ml, E) 300 µg/ml, F) 400 µg/ml, G) 500 µg/ml, and H) 600 µg/ml of concentrations

4.2.1.3 Effect of *S. articularis* L.f. Leaf Ethanol and Stem Methanol Extract on Calcium Oxalate Crystal Aggregation

Kidney stone formation is often attributed to urinary supersaturation, which occurs due to alterations in urine chemistry such as hyperoxaluria and hypercalciuria, leading to crystallization, aggregation, and eventual formation of stones (Ratkalkar and Kleinman, 2012). The inhibitory effect of *S. articularis* ethanol leaf extract on CaOx crystal formation at different concentrations are presented in **Figure 4.12,** A-H. The results showed no significant inhibitory effect. It was also observed that increasing the concentration of the extract did not lead to a reduction in the size of CaOx crystals and an increase in the inhibition percentage.

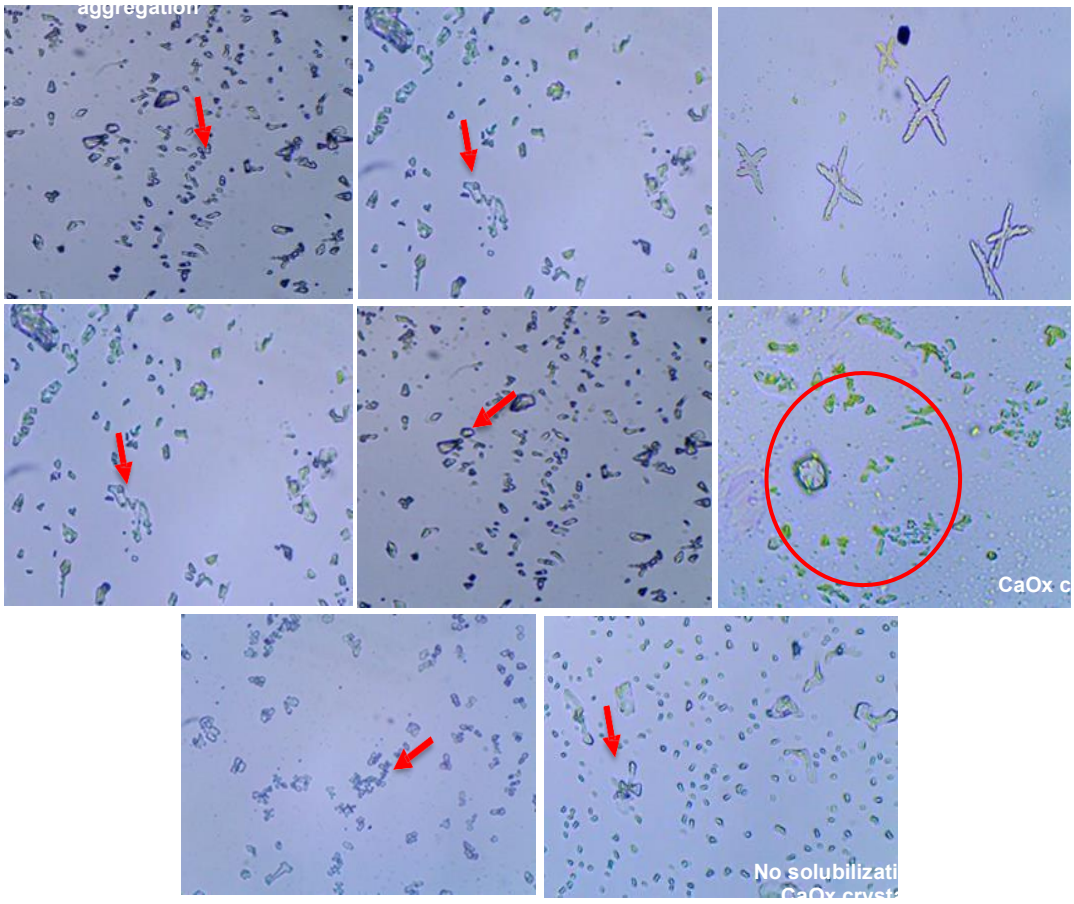

Figure 4.12. Micrographs of CaOx crystal aggregation in the absence and presence of *S. articularis* leaf ethanol extract

A) Control, B) Cystone, C) 100 µg/ml, D) 200 µg/ml, E) 300 µg/ml, F) 400 µg/ml, G) 500 µg/ml, and H) 600 µg/ml of concentrations

The stem methanol extract of *S. articularis* exhibited a significantly higher inhibitory effect of 88.4±0.002% on the CaOx crystal aggregation at 600 µg/ml than cystone, with a lower inhibitory effect of 50.21±0.004% at 100 µg/ml concentration (**Figure 4.13a**). The microscopic images displayed in **Figure 4.13b** (A-H) revealed no significant growth of crystals under the light microscope. There was a significant reduction in the size and number of crystals as extract concentrations increased from 100µg/ml to 600µg/ml, suggesting a dose-dependent inhibitory effect comparable to cystone at 600µg/ml. These findings suggested that the stem methanol extract of *S. articularis* is more effective than cystone in inhibiting the aggregation of CaOx crystals. The higher inhibitory effect of the extract indicated its potential for preventing kidney stone formation.

The stem methanol extract of *S. articularis* demonstrated a concentration-dependent inhibitory effect on CaOx crystal formation. Increasing concentrations of the extract led to a reduction in CaOx crystal size, with a corresponding increase in the inhibition percentage. In the images displayed in (A-H), an increase in crystal growth was observed under a light microscope in the negative control, followed by a significant reduction in crystal size and number in the stem methanol extract of *S. articularis*, as the concentrations increased, suggesting a dose-dependent inhibitory effect comparable to that of cystone at 600µg/ml.

Similar to the nucleation assay, the images A-H revealed that the control sample (A) without stem methanol extract of *S. articularis* and standard had the maximum number of crystals, C-H exhibited a maximum inhibition effect at various concentrations (100-600 µg/ml) when compared to cystone (B) at 600 µg/ml. The crystal formation occurred in a dose-dependent manner after 30 minutes of incubation. A constant time against various concentrations of methanol stem extract determined the rate of crystal growth in the aggregation assay experiment. The present study also exhibited strong inhibitory activity of the stem methanol extract of *S. articularis* against the crystallization of CaOx. The findings of the study are similar to earlier reports on the plants *Boldoa pupurascens* (Mosquera *et al.,* 2020)*, Ocimum bacilicum* seed extracts (Patel *et al.,* 2023), and *Daucus carota* (Bawari *et al.,* 2018).

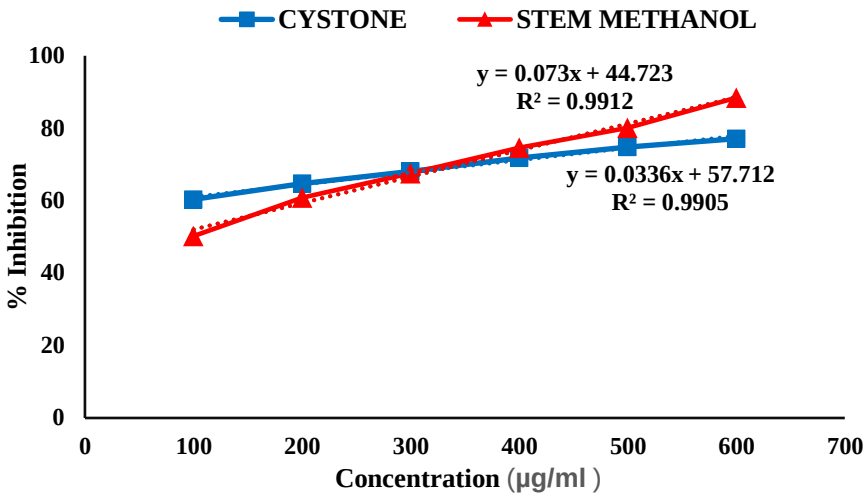

Figure 4.13a. Effect of SASM extract on CaOx crystal aggregation

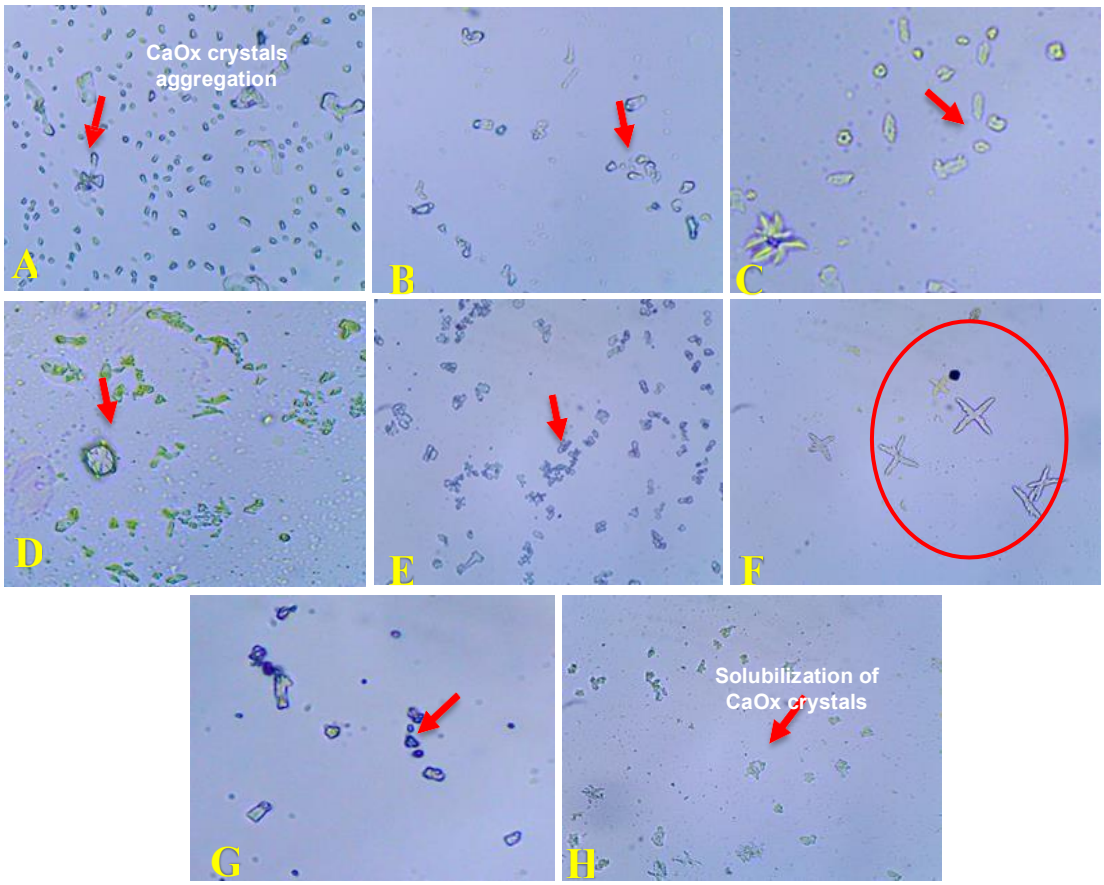

Figure 4.13b. Micrographs of CaOx crystals aggregation in the absence and presence of SASM extract

A) Control, B) Cystone, C) 100 µg/ml, D) 200 µg/ml, E) 300 µg/ml, F) 400 µg/ml, G) 500 µg/ml, and H) 600 µg/ml of concentrations

4.2.2 *In vivo* Antiurolithiatic Activity of SASM Extract

The stem methanol extract showed high inhibitory activity in *in vitro* and was chosen for further *in vivo* studies. For the *in vivo* studies, Wistar albino rats were divided into five groups: Group 1 (Control), Group II (stone-induced), Group III (Cystone treated), Group IV (SASM 250 mg/kg), Group V (SASM 500 mg/kg).

4.2.2.1 Effect of SASM Extract on Different Urine Analysis Parameters

However, treatment with extracts resulted in lower levels of calcium, phosphate, and oxalate in urine excretion. High levels of these minerals, phosphate and oxalate, contribute to the formation of calcium phosphate crystals, which create an environment with favourable conditions for stone development (Singh *et al.,* 2021). Urine with higher calcium content is more likely to precipitate and form CaOx crystals, which leads to the formation of kidney stones. Increased calcium excretion in urine and calcium deposition in the kidney in patients with renal calcium stones can be attributed to either excessive intestinal absorption or defective renal tubular reabsorption of calcium, often resulting in hyperabsorptive calcium (Xu *et al.,* 2013).

The administration of PEG in rats with induced urolithiasis (Group II) resulted in increased renal phosphate excretion and increased levels of calcium and oxalate in the urine by day 28, similar to the Group I. Animals with induced kidney stones showed significantly higher urinary levels of calcium (***$p<0.001$; 13.8±0.551), oxalate (***$p<0.001$; 12±0.374), and phosphorus (*$p<0.05$; 7.21±0.242). In contrast, rats treated with the cystone exhibited a significant decrease in calcium levels (*$p<0.05$; 7.76±0.32), oxalate (**$p<0.01$; 6.67±0.759), and phosphorus (**$p<0.01$; 5.05±0.101). Treatment with SASM low dose (LD: 250 mg/kg) did not significantly lower the elevated levels of calcium (***$p>0.001$; 10.20±0.199), oxalate (***$p<0.001$; 8.02±0.208), or phosphorus (*$p<0.05$; 5.47±0.294) in urine compared to the disease control group. A higher dose of SASM (HD: 500 mg/kg) led to a decrease in the urinary calcium, oxalate, and phosphorus (*$p<0.05$; 8.69 ± 0.214, *$p<0.05$; 5.57±0.395 and *$p<0.05$; 4.37±0.144) levels.

Rats treated with ethylene glycol exhibited a significant increase in urine BUN, creatinine, and uric acid levels compared to Group I. However, these levels were restored to normal with the SASM treatment in Groups IV and V, comparable to Group III. The levels of BUN, creatinine, and uric acid (103±7.4, 7.84±0.677, and 5.47±2.12, respectively) in the serum were highly increased (***$p<0.001$) in the stone-induced group, indicating renal impairment. However, treatment with HD SASM extract (500 mg/kg) in Group V significantly reduced the concentrations of BUN (43.9±3.54), creatinine (2.47±0.348), and uric acid (1.9±0.436) compared to Groups III and IV.

Following ethylene glycol administration, Group II showed a decrease in urinary citrate (8.89±0.248) and magnesium (1.93±0.0924) levels in comparison with the Group I. Supplementation with SASM extract in 250 and 500 mg/kg nearly normalized citrate (11.60±0.73 and17.60±0.419) and magnesium (2.32±0.0577 and 2.83±0.026) levels, respectively, and significantly increased (**$p<0.01$) these parameters (**Table 4.5**).

Magnesium levels are low in rats that are prone to stone formation, as they play a crucial role in inhibiting calcium oxalate crystal production in urine by binding to free oxalate and increasing its solubility, thus preventing crystal formation. There have been studies that suggest magnesium-containing diet interventions may help reduce the supersaturation of lithogenic salts in the urine, potentially mitigating stone formation. (Singh *et al*., 2021). Citrate, a potent inhibitor of urolithiasis, prevents the precipitation and aggregation of CaOx and phosphate by forming a soluble complex with calcium. Consistent with this, our study found that administration of the stem methanol extract of *S. articularis* and cystone increased citrate levels, which may have reduced calcium oxalate crystallization (Shah *et al*., 2012).

4.2.2.2 Effect of SASM Extract on Different Parameters of Serum and Hematology

Compared to normal groups, the lithiasis group exhibited impaired renal function due to elevated urine and serum creatinine, BUN, and uric acid levels.

The BUN, creatinine, and uric acid levels in the serum remarkably increased (153±7.26 mg/dl, 3.6±0.04, 11.7±0.586) in calculi-induced animals. On treatment with SASM (200 and 500 mg/kg), BUN, creatinine, and uric acid levels significantly decreased to 98.3±11.3 and 61±12.1 mg/dl, 1.73±0.521 and 1.03±0.393, and 7.3±0.608 and 4.93±0.913, respectively. After 28 days, hematological analysis revealed significant improvements in Group V (500 mg/kg) with increased haemoglobin (14.2±0.649), leukocytes (12.2±1.27), and erythrocyte counts (5.85±0.331), on par with Group III when compared to stone-induced groups with haemoglobin (13.7±1.3), leukocytes (11.6±0.994), and erythrocyte counts (5.45±0.319) (**Table 4.6**).

Our findings align with Kumar *et al.,* (2012), who demonstrated that *Kigelia pinnata* ethanolic extract significantly reduced creatinine and uric acid levels at the concentration of 200 mg/kg and 400 mg/kg body weight. Similarly, Vijaya *et al.,* (2013) reported that calculi-induced rats showed increased levels of BUN, creatinine, and uric acid, which were substantially lowered after treatment with *Glochidion velutinium* methanol leaf extract, supporting the potential efficacy of plant extracts in managing urolithiasis.

Studies have found that complete blood count parameters like red cell distribution width, mean platelet volume, and white blood cell count are elevated in urinary stone disease, suggesting a possible link between hematological changes and stone formation (Demiray *et al.,* 2016). These findings are consistent with a previous study of Kaleeswaran *et al*. (2019) on *Pedalium murex,* which reported a similar increase in erythrocyte count (6.21±1.02), leucocyte count (605±37.3), and haemoglobin levels (14.1±1.23).

Table 4.5. Effect of SASM extract on different parameters of urine analysis

Group	Urine Analysis (mg/dl)							
	Bun- Blood Urea Nitrogen	Creatinine	Uric acid	Oxalate	Citrate	Calcium	Magnesium	Phosphorus
Group I (Control)	18.4±1.1	1.2±0.346	0.733±0.088	4.12±0.32	22.6±0.722	7.1±0.453	3.1±0.121	5.15±0.364
Group II (Stone-induced)	103±7.4***	7.87±0.677***	5.47±2.12*	12±0.374***	8.89±0.248***	13.8±0.551***	1.93±0.0924^{ns}	7.21±0.242
Group III (Standard)	36.5±6.96^{ns}	2.47±0.467^{ns}	2±0.208^{ns}	6.67±0.759**	16.80±0.517***	7.76±0.32^{ns}	2.78±0.323	5.05±0.101
Group IV (250 mg/kg)	73.3±4.11***	5.47±0.406***	2.57±0.674^{ns}	8.02±0.208***	11.60±0.73***	10.20±0.19***	2.32±0.0577^{ns}	5.47±0.294
Group V (500 mg/kg)	43.9±3.54*	2.47±0.348^{ns}	1.9±0.436^{ns}	5.57±0.395^{ns}	17.60±0.419***	8.69±0.214*	2.83±0.026^{ns}	4.37±0.144

Values are expressed as the mean ± SD. Statistical significance (p) was calculated by one-way ANOVA followed by Dunnett's.

ns- not significant, *P< 0.05, **P< 0.01, ***P< 0.001 calculated by comparing the treated group with the control group.

Table 4.6 Effect of SASM extract on different parameters of serum and haematology in urolithiasis male wistar rats.

Group	Serum (mg/dl)			Hematological parameters		
	Bun- Blood Urea Nitrogen	Creatinine	Uric acid	RBC (X10^6/µl)	WBC (X10^3/µl)	HB (g/dl)
Group I (Control)	54.3±3.48	0.867±0.176	3.1±0.173	6.07±0.172	11.3±0.876	15.6±0.458
Group II (Stone-induced)	153±7.26***	3.6±0.040***	11.7±0.586***	5.45±0.319ns	11.6±0.994	13.7±1.3
Group III (Standard)	58.3±10.4^{ns}	1.07±0.12^{ns}	3±0.361^{ns}	6.16±0.274^{ns}	13.4±0.762	13.2±0.907
Group IV (250 mg/kg)	98.3±11.3*	1.73±0.521^{ns}	7.3±0.608**	4.86±0.4378	10±0.984	12.6±0.546
Group V (500mg/kg)	61±12.1^{ns}	1.03±0.393^{ns}	4.93±0.913^{ns}	5.85±0.331^{ns}	12.2±1.27	14.2±0.649

Values are expressed as the mean ± SD. Statistical significance (p) was calculated by one-way ANOVA followed by Dunnett's.

ns- not significant, *P< 0.05, **P< 0.01, ***P< 0.001 calculated by comparing the treated group with the control group.

4.2.2.3 Effect of SASM Extract on Animal Body and Kidney Weight

The mean body and kidney weight of the five experimental groups i.e., control (Group I), stone induced-PEG (Group II), PEG+STD (Group III), SASM-treated PEG+L.D 250 mg/kg (Group IV), PEG+H.D 500 mg/kg (Group V), recorded at the beginning of the treatment (day 1) and after 28 days are summarized in **Figure 4.14 and 4.15**. It showed that animals treated with cystone and the SASM extract (500 mg/kg) experienced a significant gain ($p<0.05$) in mean body weight compared to the stone-induced group after 28 days. This finding coincides with the previous reports of Deka *et al*. (2021), Korah *et al*. (2020), and Hiremath and Jalalpure (2016).

The results of wet kidney weight in the cystone-treated group (Group III) and SASM extract-treated groups (Group IV and Group V) were found to be similar to a regular control group. In contrast, the PEG-treated animals (Group II) showed a significant increase, indicating kidney stone formation. The kidney weight of the disease control group was greater than that of the extract-treated groups due to CaOx crystal precipitation, as reported by Sitafale *et al.* (2022). In line with Partial *et al*. (2020), our study revealed that cystone and plant extract-treated groups exhibited antiurolithiatic activity, which may have prevented stone accumulation, therefore reducing pain and consequently leading to increased food consumption and substantial weight gain. Comparable results were seen with *S. hispida* methanol extract (100 mg/kg), which showed a significant difference in body weight between the normal (192.9±4.59 mg/kg) and the cisplatin-treated group (179.3±6.10 mg/kg) ($p<0.05$) (Sitafale *et al.*, 2022). Similarly, Brancalion *et al.* (2012) found that the hydroalcoholic extract of *Copaifera langsdorffii* leaf exhibited notable antiurolithiatic activity, marked by increased body weight in extract-treated groups compared to controls.

4.2.2.4 Effect of SASM on Different Antioxidant Parameters

The total protein level significantly increased (P<0.05) to 1.89±0.552 mg/dl in the ethylene glycol-treated group (**Figure 4.16**). However, treatment with cystone and SASM extract considerably decreased the total protein level in a dose-dependent manner. The high dose 500 mg/kg (Group V), demonstrated equivalent efficacy (P<0.05) of 0.795 mg/dl to the standard treatment, cystone (0.862mg/dl).

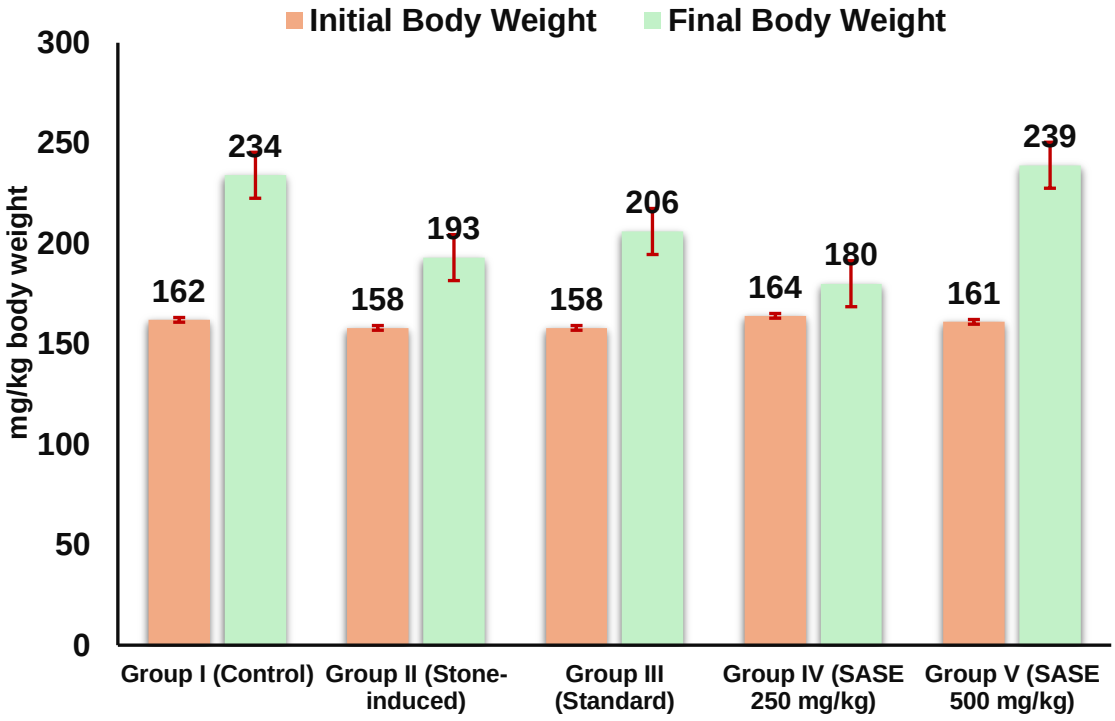

Figure 4.14 Effect of SASM extract on animal body weight

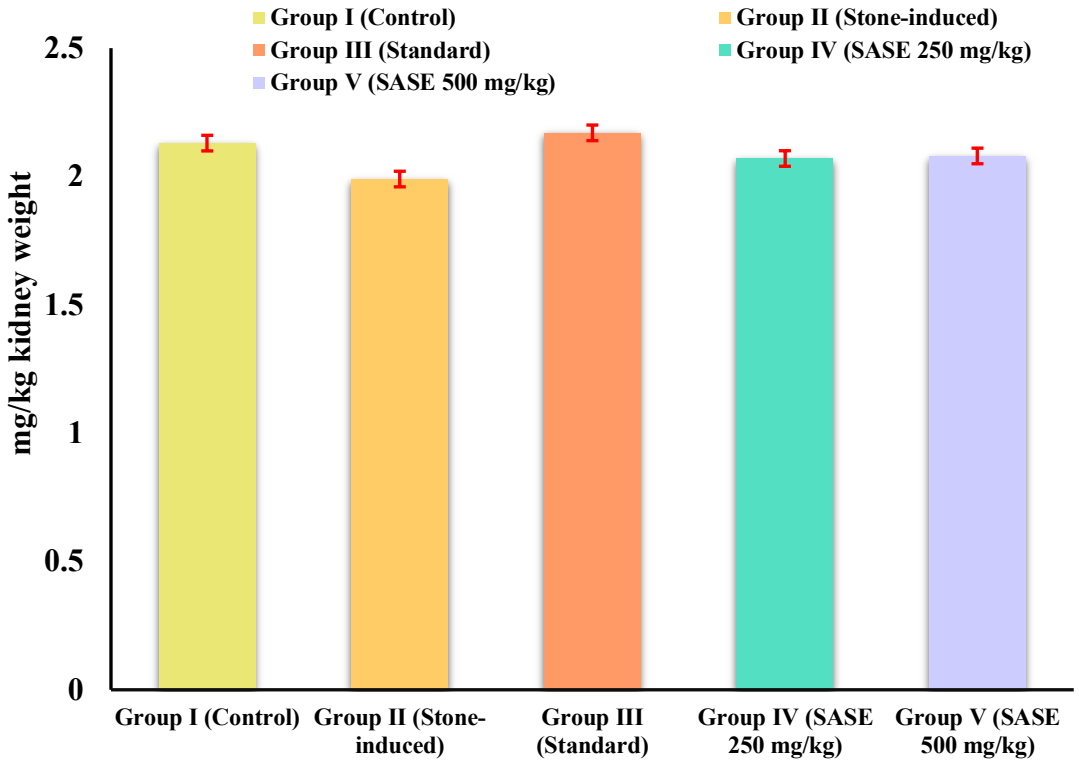

Figure 4.15. Effect of SASM extract on animal kidney weight

Values are expressed as the mean ± S.D. Statistical significance (p) was calculated by one-way ANOVA followed by Dunnett's. ns- not significant, *P< 0.05, **P< 0.01, ***P< 0.001 calculated by comparing the treated group with the control group.

In the PEG-treated lithiasis rats (Group II) an increase was observed in antioxidant enzymes including, superoxide dismutase (SOD), catalase (CAT), glutathione peroxidase (GPS), and reduced glutathione (GHS) compared to the normal control rats (Group I). The treatment with SASM HD and LD treated rats (Group IV and V), and standard cystone (Group III) maintained the antioxidant levels and reduced lipid peroxidation (LPO), when compared to the PEG-treated lithiatic rats (Group II).

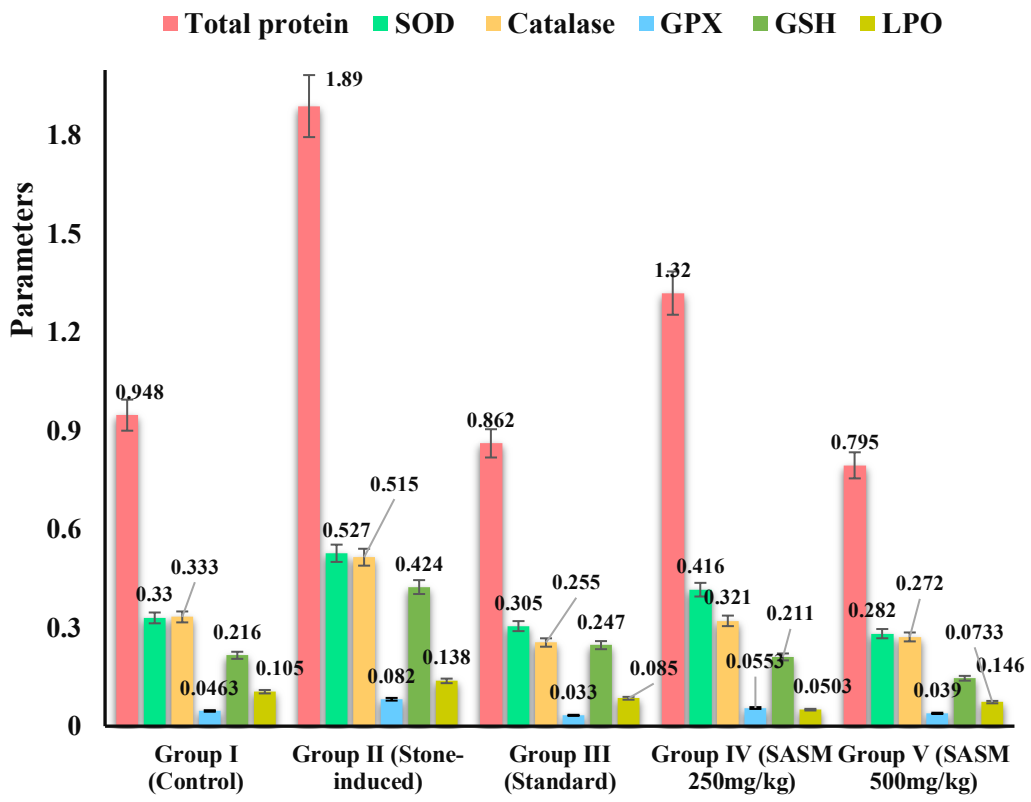

Figure 4.16. Effect of SASM on different antioxidant parameters

Values are expressed as the mean ± S.D. Statistical significance (p) was calculated by one-way ANOVA followed by Dunnett's. ns- not significant *P<0.05, **P< 0.05, ***P<0.05 calculated by comparing treated group with control group. n = 6 in each group

Thus, the 500mg/kg SASM extract treatment exhibited potent antioxidant activities in the experimental models, and increased LPO and altered GSH levels in the control group indicated that hyperoxaluria promoted extensive ROS production. The SASM extract exhibited a dose-dependent antioxidant effect, as evidenced by a significant reduction in the antioxidant levels of GSH, LPO, and catalase levels in Groups IV and V. This protective effect mitigates the toxic exposure of renal epithelial cells to oxalate, which induces lipid peroxidation (LPO) mediated by free radicals. The antioxidant response of the stem methanol extract was in a dose-dependent manner similar to previous reports of *Musa paradisiaca* pseudo stem (Panigrahi *et al*., 2017).

4.2.2.5 Histopathological Analysis of Kidney at 400X

Histopathological examination revealed significant kidney damage in urolithiasis rats exposed to PEG, characterised by large spaces, increased tubular dilation, and abnormal calcium oxalate crystal deposition. In contrast, treatment groups showed reduced crystal deposition, and less dilation was seen in the treatment groups (Groups III, IV, and V), demonstrating notable improvements. **Figure 4.17** (D & E) illustrates the treatment with the stem methanol extract of *S. articularis*. (Group-IV and V), significantly reduced calcium oxalate crystals deposition, renal tubules dilation, and interstitial inflammation compared to the PEG-treated group (Group-II). The presence of rosette-like, polycrystalline CaOx crystals indicated that these particles had adhered to and been retained within the renal tubules. Notably, the SASM extract treatment significantly decreased the CaOx crystal deposits in both urine microscopy and kidney histology.

Histological examination of kidney tissues revealed no cellular necrosis or inflammatory infiltration in the normal group, whereas PEG-treated rats showed significant inflammatory infiltrations in the renal cortex and tubular epithelium. In contrast, the SASM extract treatment resulted in a substantial reduction in inflammatory infiltration. Treatment with SASM extract-treated groups demonstrated protective effects against renal tubular necrosis score compared to the PEG-treated Group II. The cystone-treated group effectively restored urinary oxalate and calcium levels in both curative and preventive regimens, showing better results than untreated controls.

Results revealed that both the LD and HD SASM extract and standard Cystone-treated groups significantly reduced stone size and crystalluria, exhibiting considerable antiurolithiatic activity. PEG-treated rats exhibited abundant and aggregated CaOx crystal stones in their urine after 28 days. The SASM extract prevented stone formation by reducing CaOx crystal aggregation and breaking down calcium particles into smaller, invisible constituents. Through excreting a smaller amount of debris from the kidney and minimizing its retention in the urinary tract, this effect may contribute to the prevention of urinary stone formation (Neha *et al*., 2015; Kumar *et al*., 2022).

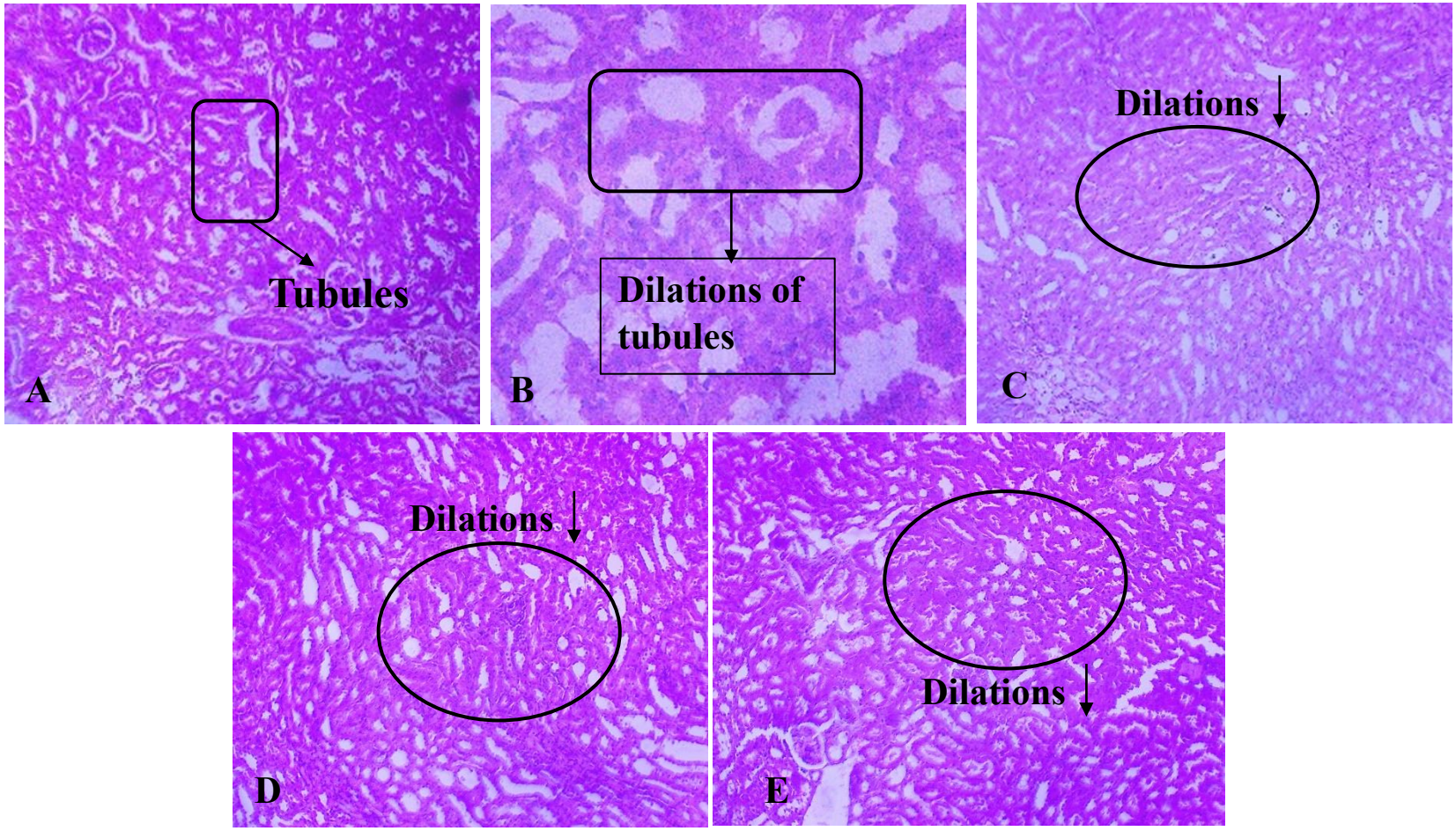

Figure 4.17 (A-E) Histopathological analysis of the kidney at 400X

A - Group I (Control), B - Group II Poly Ethylene glycol (1%) (Stone Induced), C - Group III Cystone (Standard), D - Group IV SASM extract 250mg/kg body weight and E - Group V SASM extract 500 mg/kg body weight.

4.2.3 *In vitro* Cytotoxicity Assay of SASM Extract

The *in vitro* cytotoxicity assay is essential for assessing the safety and toxicity of substances like drugs and chemicals on living cells. It helps determine cell viability, identifies potential toxic compounds, and establishes safe concentration ranges.

4.2.3.1. Brine Shrimp Lethality Assay

Table 4.7 represents data on the mortality rate of brine shrimp larvae at varying observation intervals and concentration levels of SASM extract. The plant extract exhibited low toxicity at both lower and higher concentrations, even after 24 hours of incubation, mortality rates remained minimal, with only 1-3 shrimp deaths observed at the highest concentration.

Table 4.7 Brine shrimp lethality assay

Sample Code	Concentration (µg/ml)	Mortality of Brine Shrimp (no. of. Shrimps Dead) (h)					
		1	2	4	6	24	% Mortality (at 24h)
SASM	100	0	0	0	0	0	0
	250	0	0	0	0	0	0
	500	0	1	1	1	1	3
	1000	0	0	1	1	3	10
	1500	0	0	0	0	3	10
Control $K_2Cr_2O_7$	1(mg/ml)	30	-	-	-	-	100

Values are expressed as the mean ± SD.

4.2.3.2 Cytotoxic Properties of SASM Extract Against Kidney HEK 293 Cell Line

The data presented in **Table 4.8** reveal that the crude extract exhibited 10% mortality at concentrations of 1000 µg/ml and 1500 µg/ml. The LC_{50} value was determined to be 180.00±1.8 µg/ml, indicating that the SASM extract was considered safe for therapeutic uses.

Previous studies have demonstrated the potential cytotoxicity of various plant extracts against brine shrimp larvae. Nerdy *et al.* (2021) found that the ethanolic extract of the red betel leaves exhibited toxicity against brine shrimp larvae across a range of concentrations (0 to 1000 µg/mL). Similarly, Mozibullah *et al.* (2023) reported that the leaf methanolic extracts of *Barringtonia acutangular* displayed dose-dependent cytotoxicity, with 46.24 µg/ml (LC_{50}), whereas the standard, vincristine sulfate, showed a significantly lower LC_{50}value (0.69 µg/ml). Waghulde *et al.* (2020) reported that the alcoholic and aqueous extracts of *Allium fistolisum* and *Brassica oleraceae* against brine shrimps exhibited LC_{50} values of 13.433 mg/mL and 1846.550 mg/mL, and 10.818 and 64.839 mg/mL, respectively. The different plant extracts. (*Anona muricata*, *Cymbopogon citratus*, *Gnidia pictum*, *Jatropha curcas*, and *Piper betle*) showed toxic effects on brine shrimp, with lethal time (LT_{50}) ranging from 21 to 24 hours and lethal concentration (LC_{50}) values below 1 mg/mL (Balinado and Chan, 2019).

Table 4.8 Cytotoxic properties of SASM extract against the kidney HEK 293 cell line

Test Conc. (µg/ml)	% Cytotoxicity	CTC_{50} (µg/ml)
1000	90.12±0.5	
500	89.01±3.3	
250	88.54±0.4	180.00±1.8
125	24.15±3.2	
62.5	15.58±1.7	

Values are expressed as the mean ± SD.

The phase II study demonstrated the antiurolithiatic potential of SASM extract, where *in vitro* experiments showed its ability to inhibit CaOx crystal formation, nucleation, and aggregation, the crucial steps in kidney stone development. *In vivo* studies using ethylene glycol-included urolithiasis rats,

Group V revealed that SASM extract (HD-500 mg/kg) reduced urinary levels of stone-promoting substances like calcium, oxalate, and phosphorus, while restoring protective factors like citrate and magnesium. Furthermore, SASM improved renal function, mitigated oxidative stress, and reduced kidney damage, as evidenced by histopathological analysis. Notably, cytotoxicity assay confirmed SASM's safety profile, exhibiting low toxicity in both brine shrimp larvae and human kidney cells (HEK 293), with a favorable LC_{50} value.

PHASE III

4.3 Chromatographic Profiling

Chromatographic profiling plays a crucial role in identifying and isolating bioactive compounds from plant extracts. This technique separates, identifies, and quantifies phytochemicals in plant extracts, offering valuable insights into their potential therapeutic applications. The study employed chromatographic profiling to identify and characterize bioactive compounds in *S. articularis* stem methanolic extract, focusing on terpenoids and phenolics for their known antiurolithiatic properties (El Menyiy *et al.,* 2021; Akomolafe *et al.,* 2014; Guzel *et al.,* 2021).

4.3.1 Thin Layer Chromatography Analysis

TLC was used to separate and identify terpenoids and phenolics in the SASM extract with visualization at 254nm and 366nm based on their UV absorbance. The analysis showed Rf values ranging from 0.24 to 0.98, indicating effective separation of bioactive compounds in the extract. The mobile phase comprising toluene, ethyl acetate, and formic acid (TEAF) proved optimal for the separation. The chromatogram of SASM extracts confirms the presence of terpenoids and phenolics, as shown in **Figure 4.18**. After spraying with anisaldehyde sulphuric acid reagent, the TLC plates showed bright blue- and violet-colored bands at 366nm. The TLC analysis quantified the secondary metabolites in the SASM extract, detecting terpenes and phenolics with Rf values of 0.36-0.98 (a-e) as summarized in **Table 4.9**.

Similar studies on plant extracts like *Jasminum multiflorum* have reported phytochemicals such as phenols, terpenoids, and saponins with distinct Rf values (Ganatra *et al.,* 2013). Sonam *et al.* (2013) detected alkaloids, flavonoids, tannins, and phenols in acetone, methanol, chloroform, and aqueous extracts of *Reinwardtia indica*. TLC profiling of 18 medicinal plants revealed the presence of flavonoids, saccharides, phenols, and tannins, identified by spot position and color, using spraying agents like H_2SO_4 and $FeCl_3$ (Giri *et al.,* 2020).

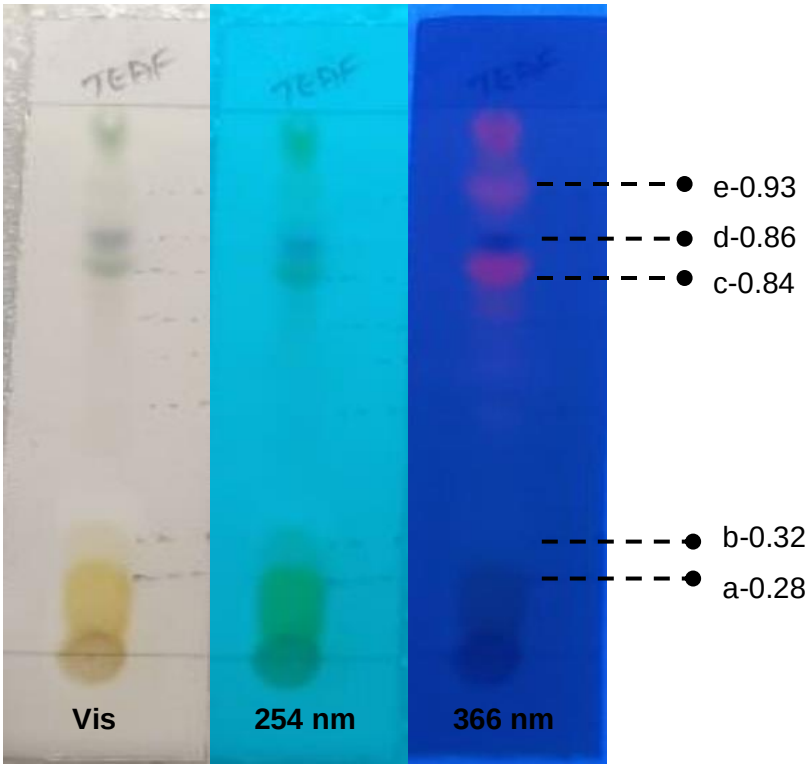

Figure 4.18 TLC profiles of SASM extract- phenolics, and terpenoids at visible light, 254 nm and 366 nm.

Table 4.9. TLC analysis of SASM Extract

Rf value obtained	Solvent system	Derivatization reagent	Inference
a-0.28 b-0.32 c-0.84 d-0.86 e-0.94	TEAF (5:5:0.5)	Anisaldehyde sulphuric acid reagent	Shades of blue, purple, or violet bands, indicate the presence of Terpenoids and Phenolic compounds

4.3.2 High Performance Thin Layer Chromatographic Analysis

Metabolic profiling using HPTLC has proven to be an effective and powerful analytical technique. HPTLC is gaining popularity due to its numerous advantages, including low mobile phase consumption, fast analysis, and the ability to analyze multiple samples simultaneously. This technique reduces analysis time and cost, and can directly handle cloudy samples and suspensions.

4.3.2.1 HPTLC Profiling for Terpenoids

HPTLC utilizes organic solvents with varying polarities to resolve and identify a wide range of chemical compounds based on their unique properties, which will also help in the characterization of bioactive compounds. The presence of various terpenoids along with other compounds at Rf values (spots a-f) of 0.095, 0.210, 0.371, 0.494, 0.531, and 0.992 in the SASM extract is presented in (**Figure 4.19).**

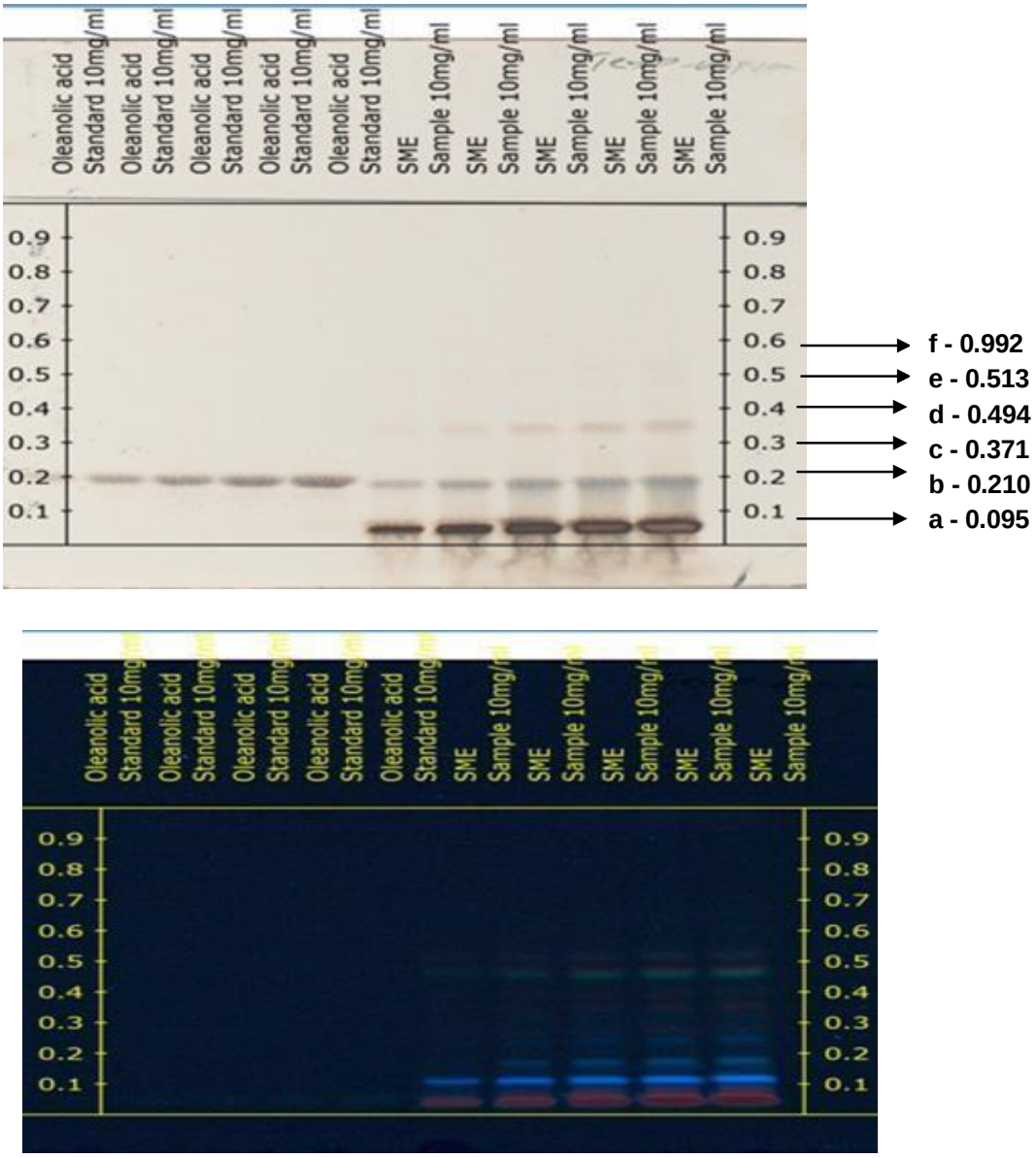

Figure 4.19. HPTLC profile showing the derivative of terpenoids

The chromatogram detected 16.96 µg/mL of terpenoids in 5 µL of SASM, confirmed before and after derivatization under both daylight and UV 366 nm. Thus, the Rf values calculated for the terpenoids present in the SASM and reference standards were compared, and from the peak area, the concentration of the terpenoids were quantified.

4.3.2.2 HPTLC Profiling for Phenolics

Phenolics have been observed in SASM extract with Rf values (spots a-g) of 0.087, 0.174, 0.490, 0.555, 0.681, 0.840, 0.877, 0.965, and 0.990, which confirms the presence of phenolics at a concentration of 13.46 µg/mL in 5 µL of extract. Chromatogram was observed under daylight as well as in ultraviolet mode, which is represented in **Figure 4.20.**

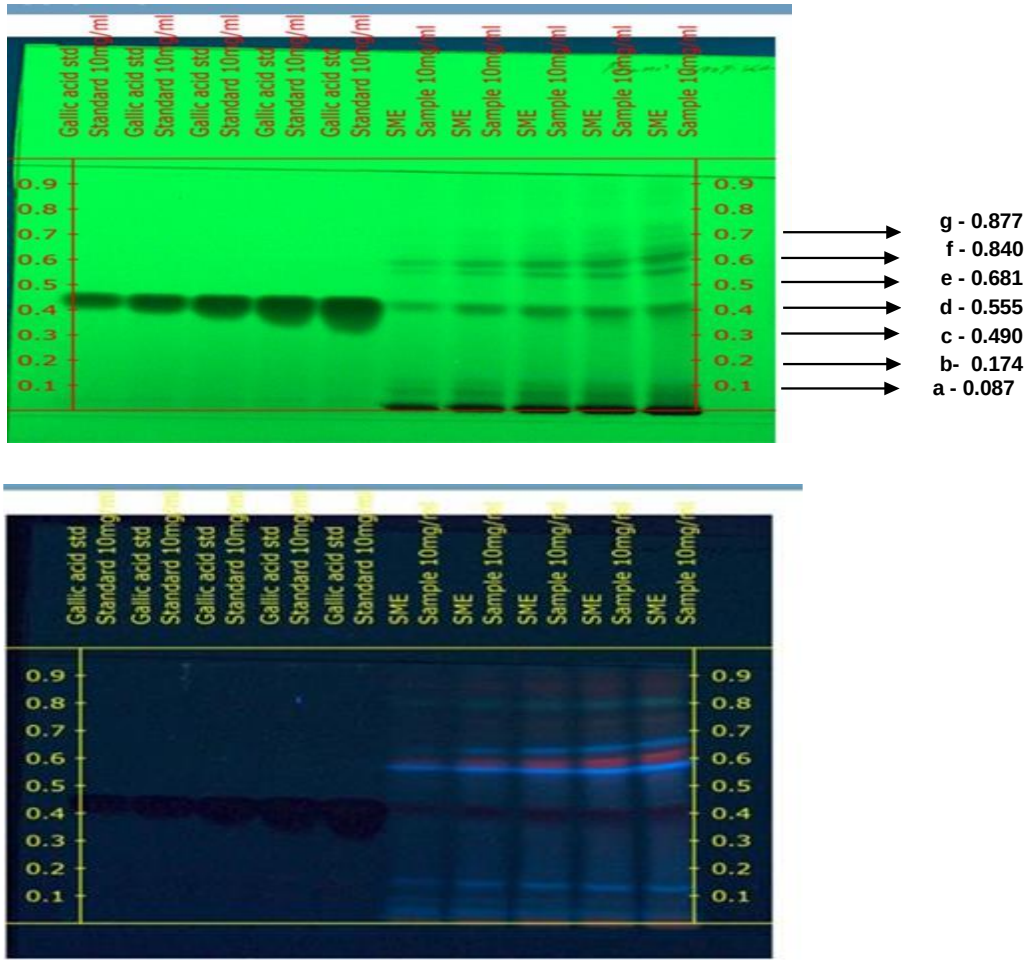

Figure 4.20. HPTLC profile showing the derivative of phenolics

The results from the HPTLC anlaysis revealed the occurrence of 11 polyvalent phytoconstituents, and the corresponding ascending order of Rf values is 0.01, 0.10, 0.18, 0.22, 0.30, 0.47, 0.53, 0.64, 0.80, 0.85, and 0.96 in *S. trifoliatus* at wavelength 366 nm for 5µL (Saraf and Saraf, 2020). The aqueous extract of *Rotula aquatica* revealed the presence of seven phenolic compounds, twelve tannins, and eleven saponins with their different Rf values (Vijayakumari *et al.,* 2016).

4.3.4 Gas Chromatographic-Mass Spectrometry Analysis

GC-MS is a powerful technique for identifying bioactive compounds in plants, combining the separation capabilities of gas chromatography with the detection power of mass spectrometry. It provides detailed information on compounds, including peak area, retention time, molecular formula, molecular weight, and structure, effectively identifying various compounds such as hydrocarbons, alcohols, acids, esters, alkaloids, and steroids.

Table 4.10 Major compounds of SASM extract from GC-MS analysis

S.No	Rt (min)	Name of Compound	Molecular Formula	Molecular wt. G/mol	Structure of the compound
1.	37.3975	Vitamin E	$C_{29}H_{50}O_2$	430.7	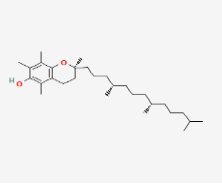
2.	36.7290	Hentriacontane	$C_{31}H_{64}$	436.8	

S.No	Rt (min)	Name of Compound	Molecular Formula	Molecular wt. G/mol	Structure of the compound
3.	36.2769	Pyrolo[3,2-d]pyrimidin-,4(1H,3H)-dione	$C_6H_5N_3O_2$	151.12	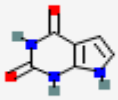
4.	36.0841	Gamma.-Tocopherol	$C_{28}H_{48}O_2$	416.7	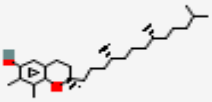
5.	36.0835	1H-indole, 3,3'-[1,4-phenylenedi-2,1-ethenediyl]bis[1,2-dimethyl-	$C_{30}H_{28}N_2$	416.6	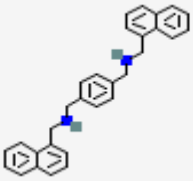
6.	35.4949	Triacontane	$C_{30}H_{62}$	422.8	
7.	34.3266	2-Amino-4-(1-ethylpropyl)-4H-benzo[h]chromene-3-Carbonitrile	$C_{19}H_{20}N_2O$	292.4	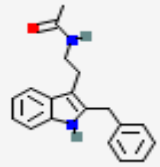
8.	34.1774	α-Tocospiro B	$C_{29}H_{50}O_4$	462.7	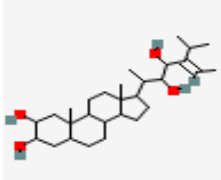

S.No	Rt (min)	Name of Compound	Molecular Formula	Molecular wt. G/mol	Structure of the compound
9.	33.8857	Squalene	$C_{30}H_{50}$	410.7	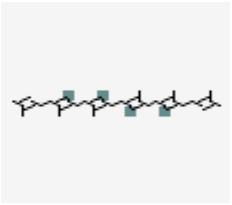
10.	33.5846	Octacosane	$C_{28}H_{58}$	394.8	
11.	33.0651	Isobutyl octadecyl ether	$C_{22}H_{46}O$	326.6	
12.	32.9906	Octadecanoic acid, 2,3-dihydroxypropyl ester	$C_{21}H_{42}O_4$	358.6	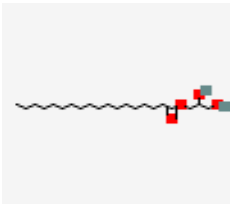
13.	32.6197	(E)-3,3'-Dimethoxy-4,4'-dihydroxystilbene	$C_{16}H_{16}O_4$	272.29	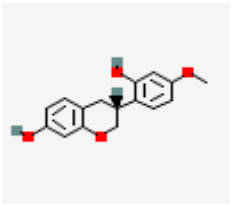
14.	32.6032	n-Butyric acid tetrahydrofurfuryl ester	$C_8H_{14}O_3$	158.19	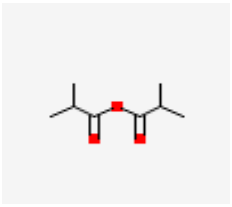

S.No	Rt (min)	Name of Compound	Molecular Formula	Molecular wt. G/mol	Structure of the compound
15.	32.5916	Spiro[bicyclo[2.2.1]hepta ne-2,2'-[1,3]dioxolane]-3- one, 1,7,7-trimethyl-	$C_{12}H_{18}O_3$	210.27	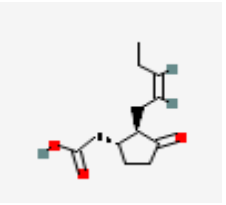
16.	32.2909	Isobutyl hexadecyl ether	$C_{20}H_{42}O$	298.5	
17.	32.2081	Succinic acid, 3-methylbut-2-en-1-yl diphenylmethyl Ester	$C_{22}H_{24}O_4$	352.4	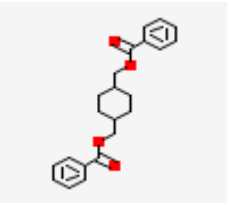
18.	32.2081	Pyridine, 4-tert-butyl-2-(tert-butylthio)-	$C_{13}H_{21}NS$	223.38	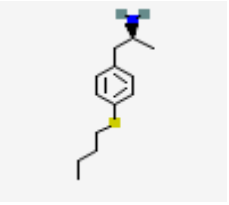
19.	32.0856	Hexadecane, 1-iodo-	$C_{16}H_{33}I$	352.34	
20.	32.0854	Heptacosane	$C_{27}H_{56}$	380.7	

S.No	Rt (min)	Name of Compound	Molecular Formula	Molecular wt. G/mol	Structure of the compound
21.	32.0239	Heneicosane	$C_{21}H_{44}$	296.6	
22.	32.0236	Hexacosane	$C_{26}H_{54}$	366.7	
23.	31.8177	Silicon tetrafluoride	F_4Si	104.079	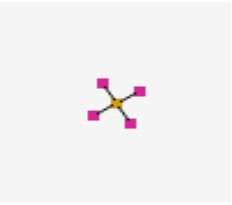
24.	31.6710	Phthalic acid, di(2-propylpentyl) ester	$C_{24}H_{38}O_4$	390.6	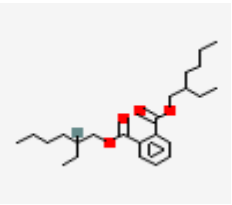
25.	31.4920	2-Methyltetracosane	$C_{25}H_{52}$	352.7	
26.	31.4894	5-Methyl-4-hexene-1-yl acetate	$C_9H_{16}O_2$	156.22	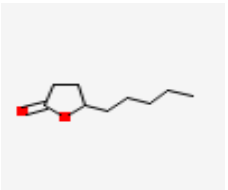

S.No	Rt (min)	Name of Compound	Molecular Formula	Molecular wt. G/mol	Structure of the compound
27.	31.4869	Isobutyl hexadecyl ether	$C_{20}H_{42}O$	298.5	
28.	31.3367	Hexadecanoic acid, 2-hydroxy-1-(hydroxymethyl)ethyl ester	$C_{19}H_{38}O_4$	330.5	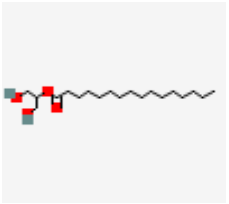
29.	31.1995	Pentacosane	$C_{25}H_{52}$	352.7	
30.	30.9414	3,5-Diamino-1,2,4-triazole	$C_2H_5N_5$	99.1	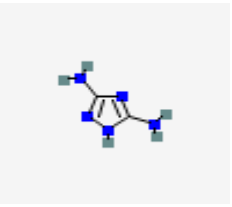
31.	30.6426	Heptadecane	$C_{17}H_{36}$	240.5	
32.	30.6336	Docosyl isobutyl ether	$C_{26}H_{54}O$	382.7	

S.No	Rt (min)	Name of Compound	Molecular Formula	Molecular wt. G/mol	Structure of the compound
33.	30.6154	13-Docosen-1-ol, (Z)-	$C_{22}H_{44}O$	324.6	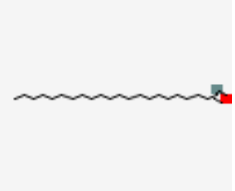
34.	24.562	Guanozole	$C_2H_5N_5$	99.1	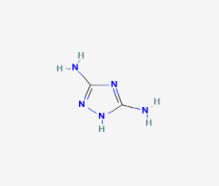
35.	20.411	Catechol	$C_6H_6O_2$	110.11	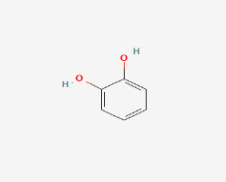
36.	18.2376	Vanillin	$C_8H_8O_3$	152.15	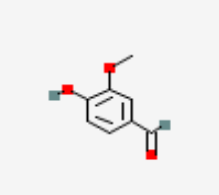
37.	17.2378	Nicotinic acid	$C_6H_5NO_2$	123.11	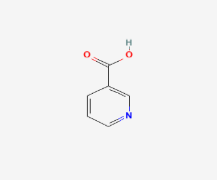
38.	10.9371	D-Mannitol	$C_6H_{14}O_6$	182.17	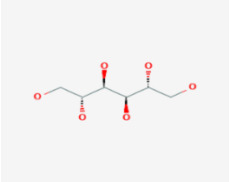
39.	10.8040	Maltol	$C_6H_6O_3$	126.11g/mol	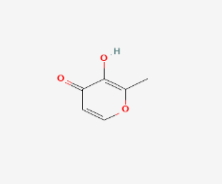

S.No	Rt (min)	Name of Compound	Molecular Formula	Molecular wt. G/mol	Structure of the compound
40.	7.2068	Furfurylmethylamphetamine	$C_{15}H_{19}NO$	229.32	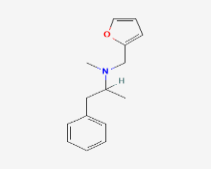

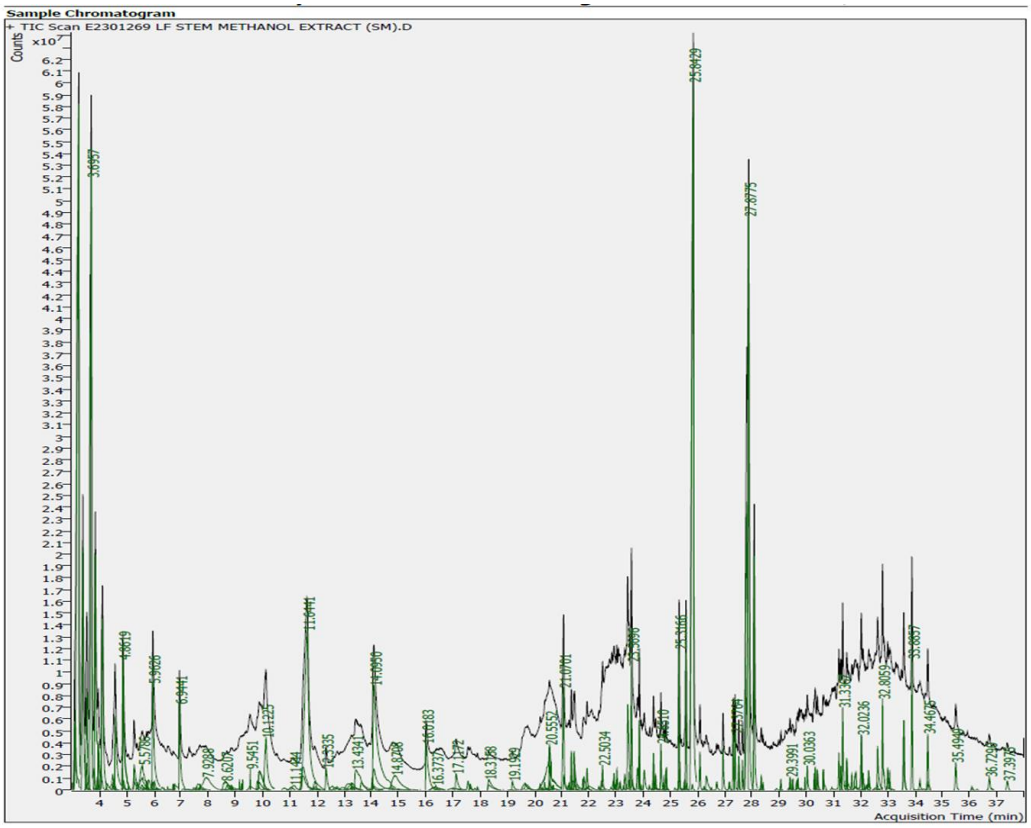

Figure 4.21 GC-MS spectral analysis of SASM Extract

The GC-MS analysis showing the relative concentrations of various compounds eluting at differential retention times, which are present in the SASM extract, was depicted in **Figure 4.21**. The mass spectrometer analyses the compounds eluted at different times, breaking them down into smaller fragments, which produce peaks at distinct mass-to-charge (m/z) ratios, allowing for the

compound's nature and structure. In **Table 4.10**, the GC-MS analysis of 40 compounds and their retention time, molecular weight, molecular formula, and structure were displayed. The retention time of 40 compounds ranged from 7.2068 to 37.3975. Among these, 12 key compounds were identified based on maximum peak area and retention time, including Vitamin E (RT-37.397), Hentriacontane (RT-36.729), Pyrolo(3,2-d)pyrimidin-2,491H,3H)-dione (RT-36.2769), gamma-tocopherol (RT-36.0841), 1H-indole,3,3'-[1,4-phenylenedi-2,1-ethenediyl]bis[1,2-dimethyl (RT-36.0835), Triacontane (RT-35.4949), 2-Amino-4-(1-ethylpropyl)-4H benzo[h]chromene-3-Carbonitrile (RT-34.3266), alpha-tocospiro B (RT-34.1774), Squalene (RT-33.8857), octasone (RT- 33.5846). isobutyl octadecyl ether (Rt-33.0651), listed in descending order of retention time.

The GC-MS analysis of *Spermacoce articularis* whole plant ethanol extract revealed 25 compounds, with major compounds including 2-Benzylidene-3-oxo-4-(octylsulfany1)-2,3-dihydrothiophene-1 dioxide, Tridecanoic acid, and 3,7-Dimethyl-3-hydroxy-4-isopropyl-6-octadiene (Soosairaj *et al.,* 2013). *Mussaenda frondosa* whole plant ethanol extract was found to contain four major compounds, including (-)-Quinic acid, 4-((1E)-3-hydroxy-1-propenyl)-2-methoxyphenol, 1,2,3-benzenetriol, and Naphthalene, decahydro-2-methoxy- (Gopalakrishnan and Vadivel, 2011). Similarly, *Ipomoea sepiaria* ethanol leaf extract was found to contain 20 compounds, including alkanes, alkenes, fatty acids, and sterols, such as squalene, campesterol, stigmasterol, and β-sitosterol (Senthil *et al.,* 2016).

The results of chromatographic profiling of SASM extract in phase III revealed the presence of various bioactive compounds. TLC and HPTLC analysis detected terpenoids and phenolics with distinct retention factor (Rf) values. HPTLC fingerprinting confirmed the presence of 16.96 µg/mL of terpenoids and 13.46 µg/mL of phenolics in the extract. From the GC-MS analysis of identified 40 compounds, catechol, phthalic acid, Vitamin E, D-mannitol, gamma-tocopherol, squalene, and nicotinic acid were identified as major compounds with retention times ranging from

7.2068 to 37.397 minutes. These findings provide valuable insights into the phytochemical composition of *S articularis* and support its potential therapeutic applications.

PHASE IV

4.4 *In Silico* Analysis of Anti-Urolithiatic Activity

4.4.1 Molecular Docking Studies Against Urolithiasis Receptors

Molecular docking is a computational method that aids in structure-based drug design, which predicts the interaction of potential lead compounds with targets and unravels the underlying molecular mechanisms of inhibitory activity against diseases.

In this phase, three entry-level urolithiasis receptors, like Tamm-Horsfall protein, calcium oxidoreductase enzyme, and calcitonin hormones, were selected to conduct molecular docking studies using the identified ligands from the SASM extract. The 3D structure and information of the three receptors which is responsible for urinary stone formation are depicted in Figure 4.22.

Tamm-Horsfall protein (THP), also known as uromodulin, produced in the kidneys. inhibits the crystallization of calcium oxalate, thus preventing kidney stone formation and urinary tract infections at low ionic strength (Lopez *et al.* 1986; Scur and Robertson, 1986). Calcium oxidoreductase enzyme is a primary factor in urinary stone formation and also plays a vital part in numerous enzymatic processes and kidney function. This enzyme mainly participates in calcium metabolism, and their excessive levels can result in the formation of CaOx crystals. The hormone, calcitonin, produced by the thyroid gland, inhibits bone resorption by regulating the levels of calcium and phosphorus in the blood, and may influence renal calcium, potentially influencing stone formation (Pivari *et al.,* 2019). Finding potential compounds from the SASM extract that target THP, calcium oxidoreductase, and calcitonin could lead to the development of new therapies for preventing kidney stones.

From GC-MS analysis, 25 key compounds belonging to phenolics, terpenoids, and sugar derivatives were identified based on the highest peak area and subjected to docking studies to assess their efficacy in treating urinary stones with these three receptors. The docking interaction of SASM extract compounds with the receptor Tamm-Horsfall protein revealed binding affinity ranging from -

6.406 kcal/M to -3.684 kcal/M (**Figure 4.23a**). D-mannitol showed the highest binding affinity of -6.406 kcal/M followed by vanillin (-4.065 kcal/M), 2,6-Dimethoxy-4-vinylphenol (-3.954 kcal/M), Squalene (-3.913 kcal/M), Catechol (-3.864 kcal/M) and Beta-Sitosterol (-3.684 kcal/M) while the standard cystone exhibited -5.988 kcal/M of binding affinity. Type of interaction and residue information are represented in **Table 4.11.**

a) Cryo-EM of native human uromodulin (UMOD)/Tamm-Horsfall protein (THP) filament

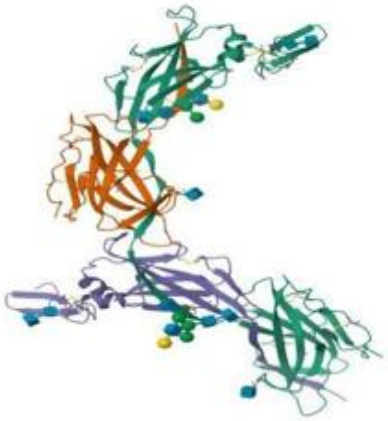

PDB ID- 6TQK

Chains ABC

Sequence length 563

b) Calcium Oxidoreductase

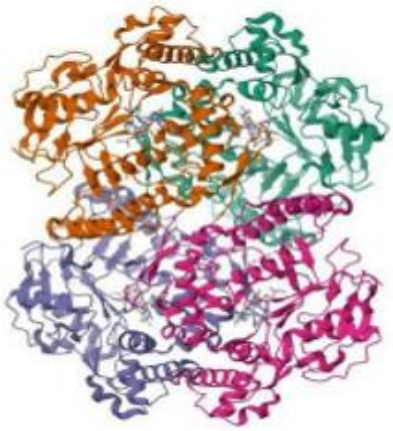

PDB ID-4V3U

Chains ABCD

Sequence length 420

C) Human Calcitonin Receptor

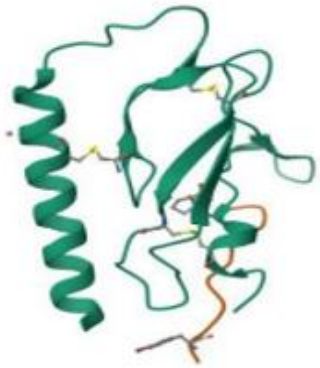

PDB ID-5II0

Chains ABC

Sequence length 120

Figure 4.22. Receptors responsible for urolithiasis.

Table 4.11. Binding interactions of urolithiasis receptors and phytocompounds

PubChem ID	Ligand	Docking Score kcal/M	Interaction	Residue information
		Tamm Horsfall- 6TQK		
6251	D-mannitol	-6.406	H-bond	C: SER 426
1183	Vanillin	-4.065	H-bond	C: SER 426, A: ARG 449
35960	2,6-Dimethoxy-4-vinylphenol	-3.954	H-bond	C: SER 426, A: ARG 449
638072	Squalene	-3.913	H-bond, Pi-Cation, Salt bridge	-
289	Catechol	-3.864	H-bond, Pi-Cation, Salt bridge	-
222284	Beta-Sitosterol	-3.684	H-bond	-
156963329	Cystone	-5.988	H-bond	C: SER 426, A: ARG 449
		Calcium oxidoreductase- 43VU		
6251	D-mannitol	-7.289	H-bond, Pi- Cation, Salt bridge	A: GLU 333, THR 332, B: CYS 302, GLH 333, D: GLH 333, SIS 302, C: GLU 333, HIP 346
26762	Furfurylmethylamphetamine	-5.556	H-bond	A: GLU 333
289	Catechol	-4.99	H-bond, Salt bridge	B: CYS 302, GLH 333
15078	Guanazole	-4.638	H-bond	A: GLU 333, B: GLH 333, SIS 302, D: SIS 302
35960	2,6-Dimethoxy-4-vinyl phenol	-4.577	H-bond, Pi- Cation, Salt bridge	-
1183	Vanillin	-4.323	H-bond, Salt bridge	C: HIP 346, B: CYC 302, D: CYS 302
156963329	STD-Cystone	-6.026	H-bond	-
		Calcitonin- 5II0		
6251	D-mannitol	-8.41	H-bond	A: TYR 92, SER 91, B: ARG 45
26762	Furfurylmethylamphetamine	-6.363	H-bond	A: ASP 83
938	Nicotinic acid	-5.995	H-bond	A: ASP 83, B: ARG 45
289	Catechol	-5.577	-	-
638072	Squalene	-5.545	-	-
94378	6 Gingerone	-5.363	H-bond	A: ASP 83
1183	Vanillin	-4.877	H-bond	A: ASP 83
1017	Phthalic acid	-4.57	H-bond, Salt bridge	A: PHE 94, LYS 107, B: LYS 46
8369	Maltol	-4.526	H-bond	A: ASP 83, B: ARG 45
92729	gamma-Tocopherol	-4.284	H-bond	A: ALA 87
156963329	STD-Cystone	-7.752	-	-

2D Interaction	3D Interaction
Tamm Horsfall protein-6TQK	
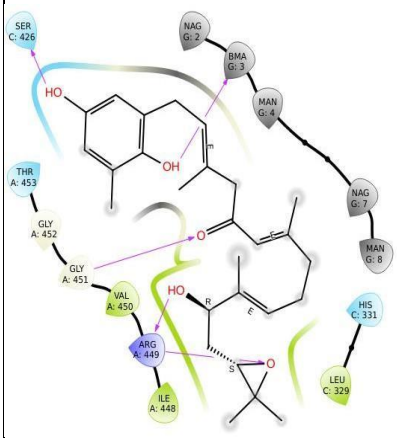	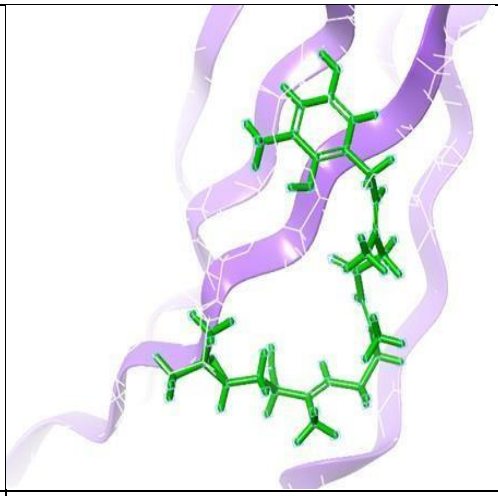
Cystone	**DS: -5.98862 kcal/M**
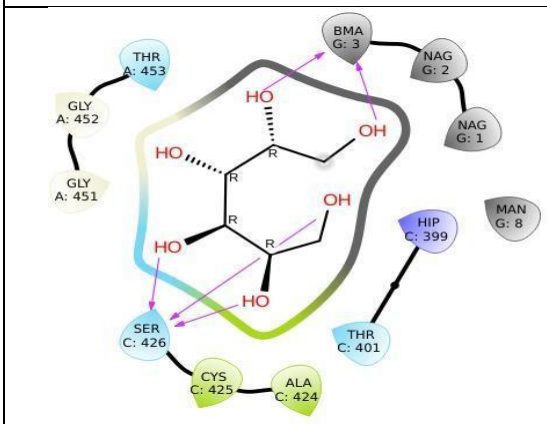	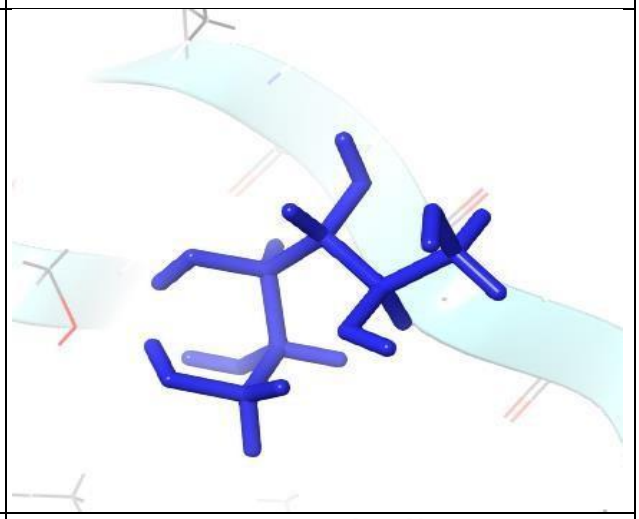
D-mannitol	**DS: -6.406 kcal/M**
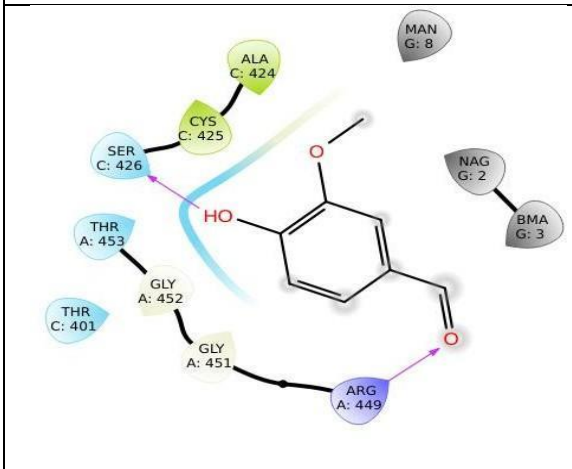	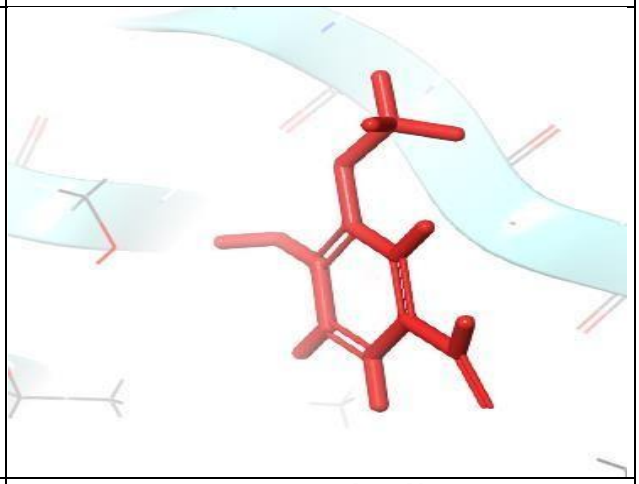
Vanillin	**DS: -4.065 kcal/M**

Figure 4.23. a) Binding interactions of Tamm-Horsfall with Cystone and phytocompounds

2D Interaction	3D Interaction
Calcium oxidoreductase- 43VU	
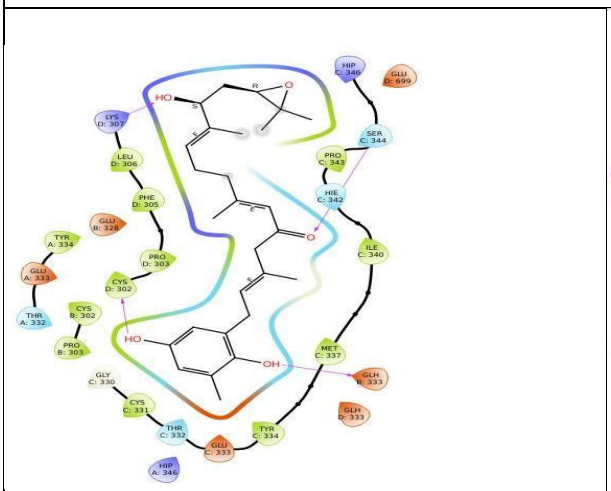	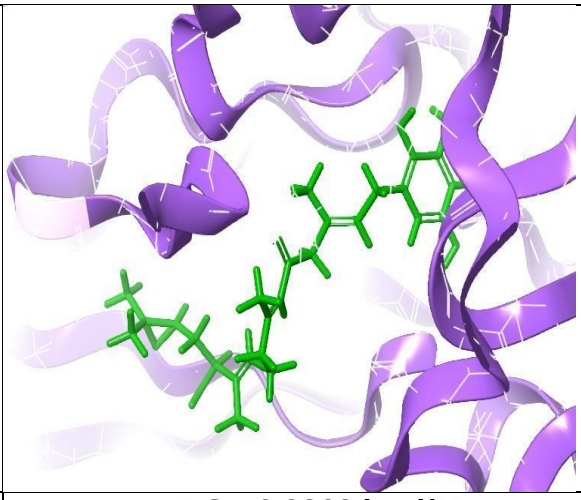
Cystone	**DS: -6.0269 kcal/M**
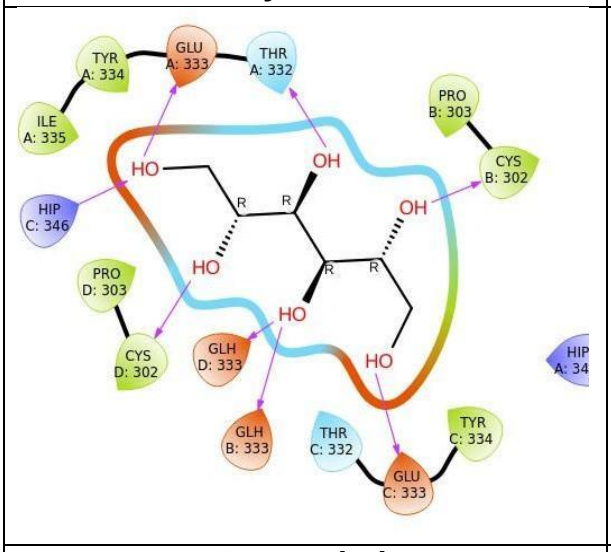	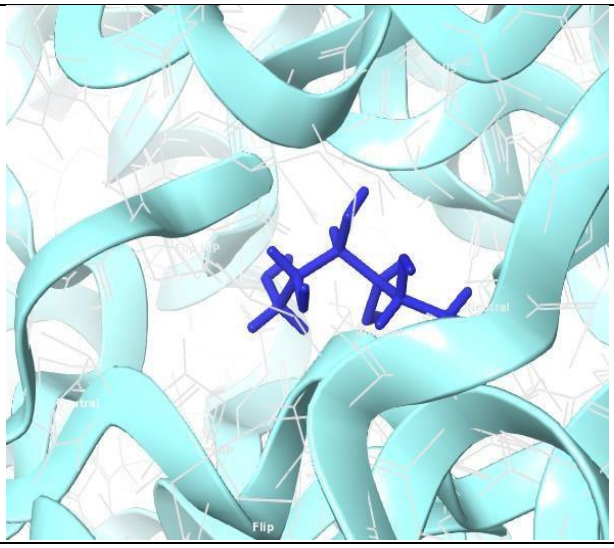
D-mannitol	**DS: -7.289 kcal/M**
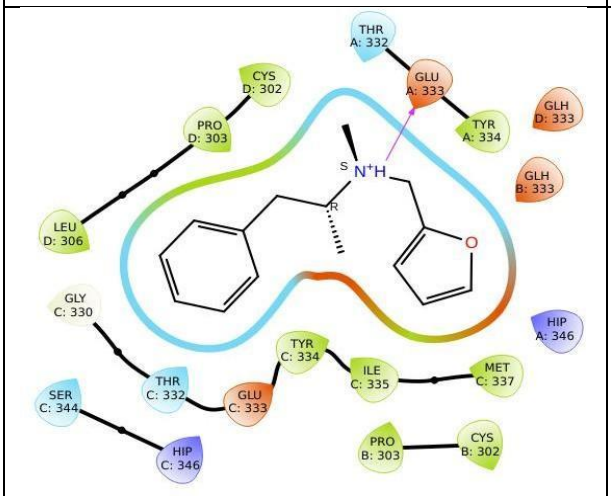	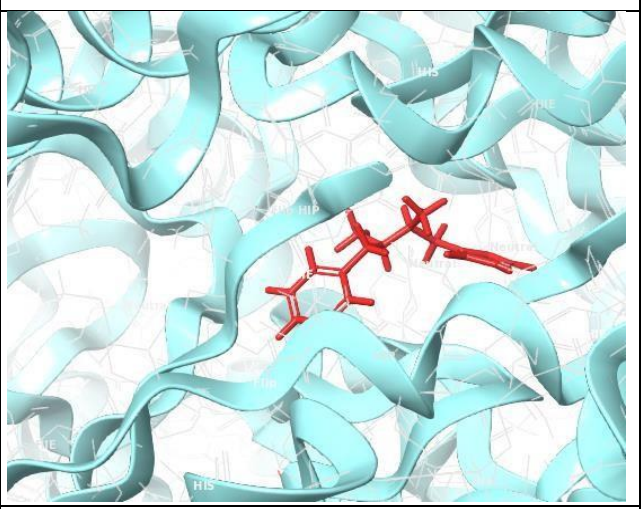
Furfurylmethylamphetamine	**DS: -5.556 kcal/M**

Figure 4.23. b) Binding interactions of calcium oxidase with Cystone and phytocompounds

2D Interaction	3D Interaction
Calcitonin- 5ll0	
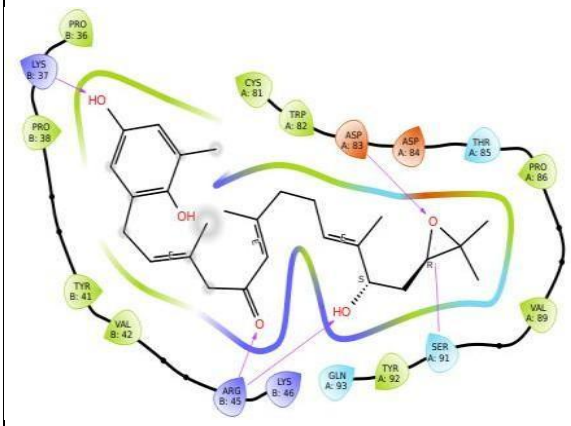	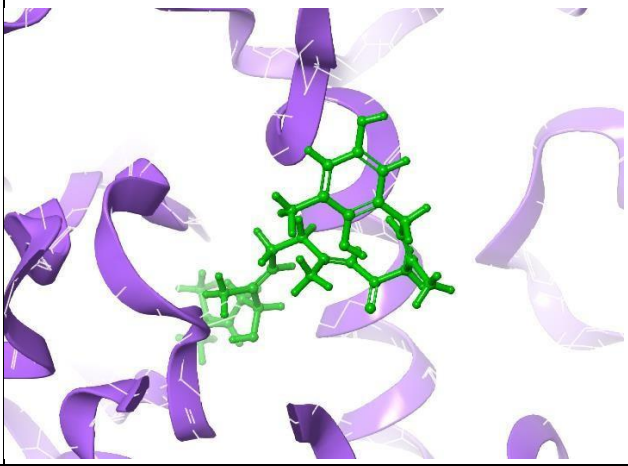
Cystone	**DS: -7.7528 kcal/M**
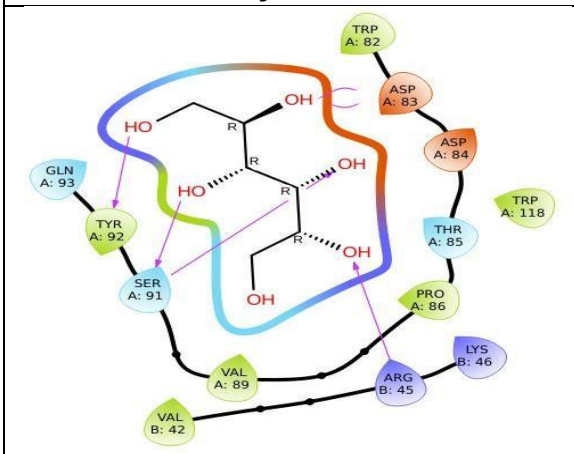	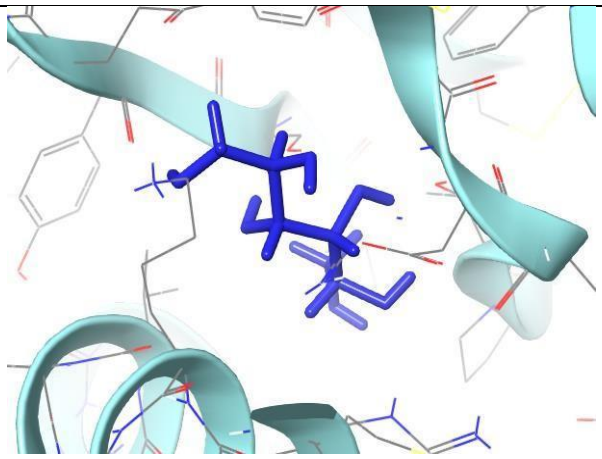
D-mannitol	**DS: -8.410 kcal/M**
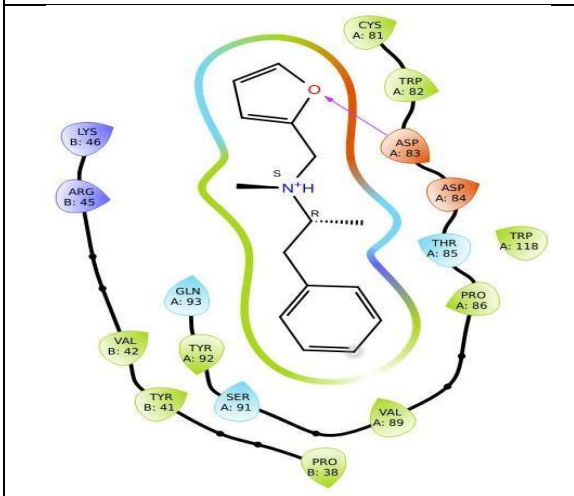	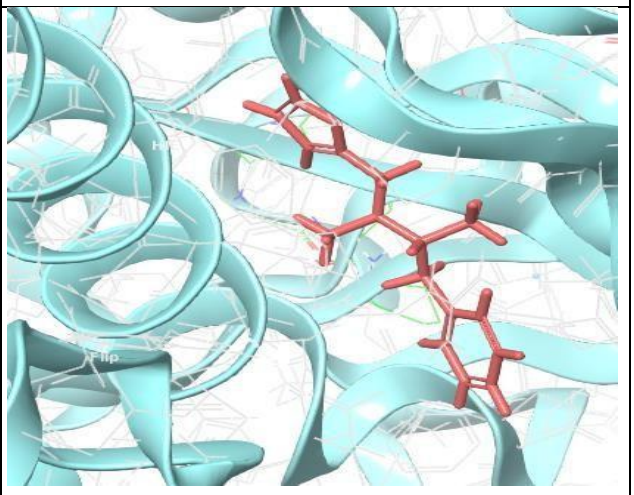
Furfurylmethylamphetamine	**DS: -6.363 kcal/M**

Figure 4.23. c) Binding interactions of calcitonin with Cystone and phytocompounds

The binding affinity of Calcium oxide reductase enzyme ranges from -7.289 kcal/M to -4.323 kcal/M (**Figure 4.23b**). D-mannitol showing the strong binding affinity of -7.289 kcal/M followed by furfuryl methylamphetamine (-5.556 kcal/M), Catechol (-4.99 kcal/M), Guanazole (-4.638 kcal/M), 2,6-Dimethoxy-4- vinyl phenol (-4.577 kcal/M), Vanillin (-4.323 kcal/M), while the standard cystone exhibited -6.026 kcal/M of binding affinity (Table 14). The docking results of the receptor calcitonin hormones revealed binding affinity ranging from -8.41 kcal/M to -4.284 kcal/M (**Figure 4.23c**). Likely, D-mannitol showed the highest binding affinity of -8.41 kcal/M followed by furfurylmethylamphetamine (-6.363 kcal/M), Nicotinic acid (-5.995 kcal/M), Catechol (-5.577 kcal/M), Squalene (-5.545 kcal/M), 6-Gingerone (-5.363 kcal/M), while the standard cystone exhibited -7.752 kcal/M of binding affinity (**Table 4.11**).

The role of D-mannitol in treating kidney stones has been a subject of debate, with conflicting findings reported in earlier research. Research from the 1980s and 1990s suggested that sugar alcohols like D-mannitol may enhance the risk of developing CaOx stones (Anderson, 1982; Reiser, 1978; Rushton *et al.,* 1981). However, recent research has shed new light on the potential benefits of D-mannitol in kidney stone treatment. Recent research has highlighted D-mannitol's diuretic properties, which can promote the excretion of toxic materials and protect against nephrotoxicity (Nagavalli *et al.,* 2023). In addition, previous studies have reported the beneficial effects of D-mannitol in scavenging the free radical-induced injury and kidney transplantation (Laar, Schouten, Ijzermans *et al.,* 2021; Boland and Garland, 1993). These recent findings are in accordance with our results, which help to understand the role of D-mannitol in urolithiasis treatment, revealing its potential therapeutic benefits. The conflict between earlier and recent research suggests the need for further research to explore its effect on urolithiasis and other ailments.

4.4.2. Molecular Dynamics Simulation

Molecular dynamics simulation (MDS) is an *in silico* method employed to predict the dynamic behaviour and stability of the protein-ligand docked complex over a specific time, with specific temperature, volume, and pressure (Salo-ahen *et al.,* 2021). The current study incorporated MDS to probe the docking interaction of

the top-scored compound D-mannitol with the calcitonin hormone, which possesses a binding affinity of -8.4 kcal/M. The simulation spanning 100 nanoseconds explored the molecular flexibility, stability, and structural behavior of the docked protein-ligand complex.

The root mean square deviation (RMSD) values of protein Cα, backbone, and heavy atoms were initiated at 1.5 Å at 0 ns and then stayed stable up to the narrow range of 2.8 Å till 30 ns and maintained a stabilized complex from 42ns to 100 ns at 5 to 7 Å. This indicated lesser fluctuations in protein structure during MD simulation shown in **Figure 24**. The blue spectrum depicts the protein α-carbon backbone corresponds to X-axis which represents simulation time in nanoseconds (ns), while the red spectrum represents the ligands that corresponds to Y-axis, which is measured in angstroms (Å).

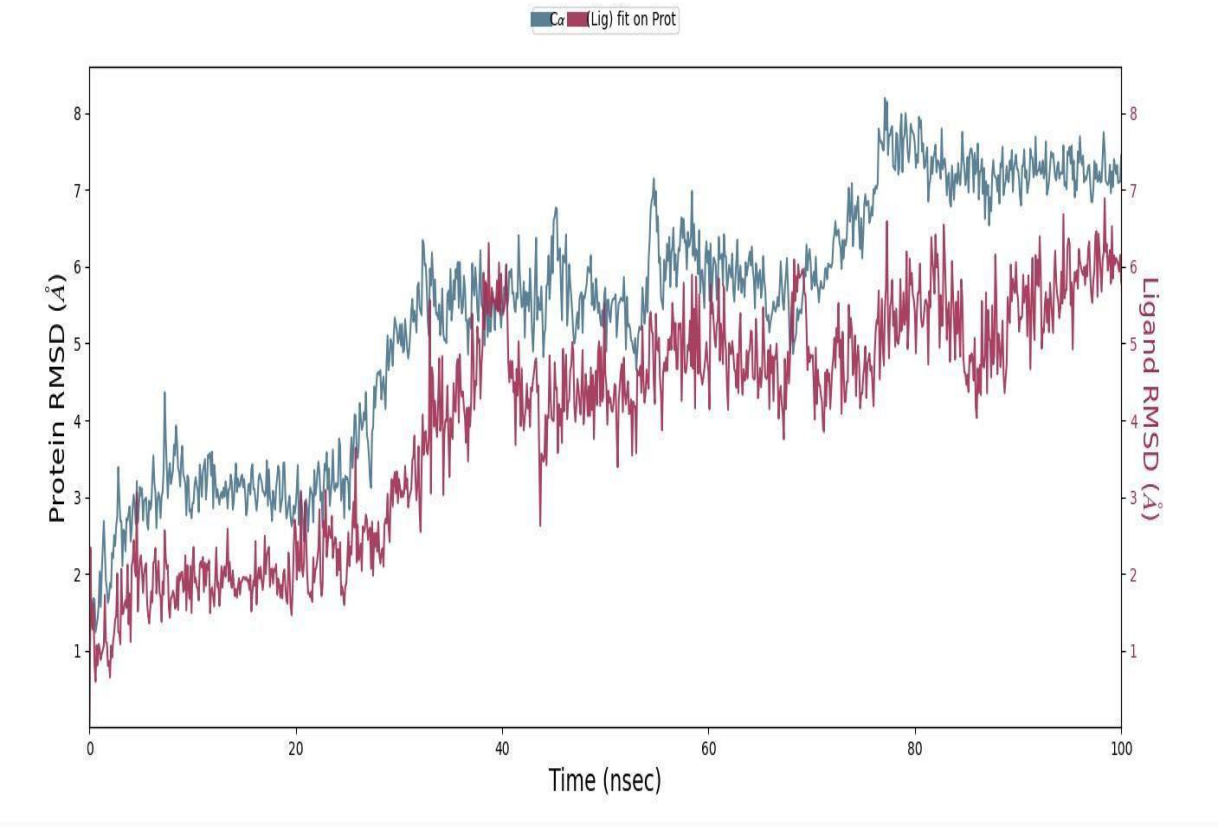

Figure 4.24: RMSD plot of calcitonin and D-mannitol complex

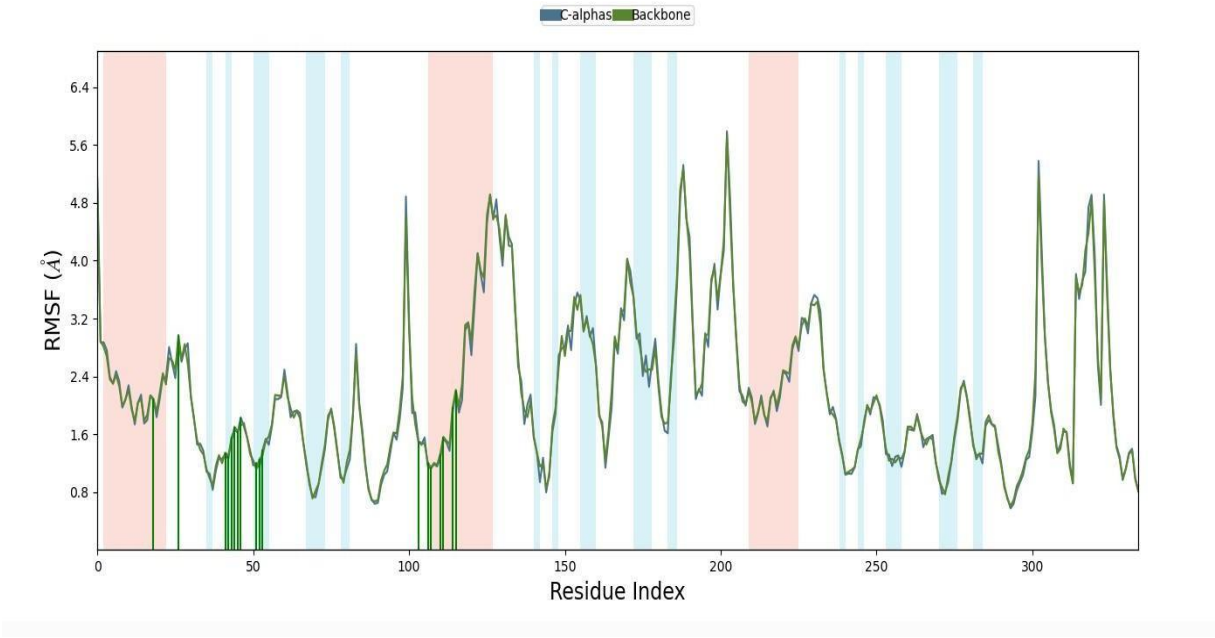

Figure 4.25. RMSF plot of calcitonin and D-mannitol complex

RMSF plot represents the alpha carbon of the protein's backbone, and (green bar) the ligands make contact with the protein.

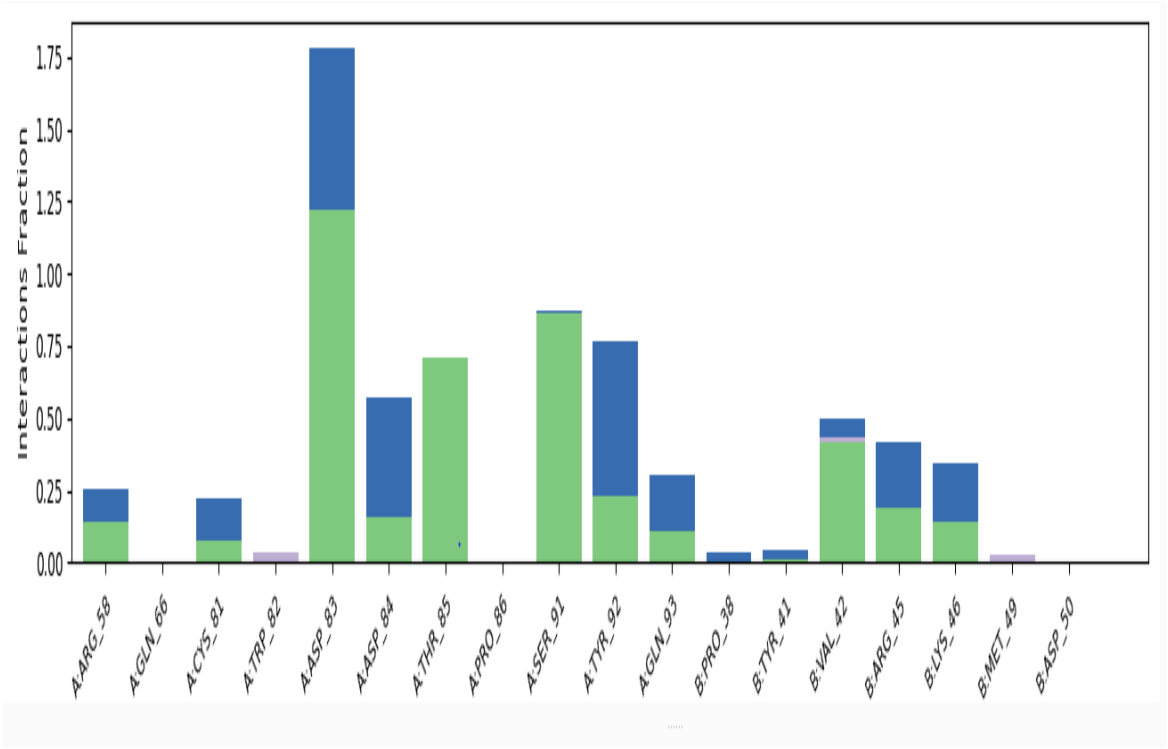

Figure 4.26. Count of interaction in histogram form of calcitonin and D-mannitol

The histogram shows the number of amino acids interacting with D-mannitol, and the interactions were indicated as strong green H-bonds, lavender hydrophobic bonds, and blue water bridges. X-axis- Position of amino acids in the protein, Y-axis- Interaction fraction scale.

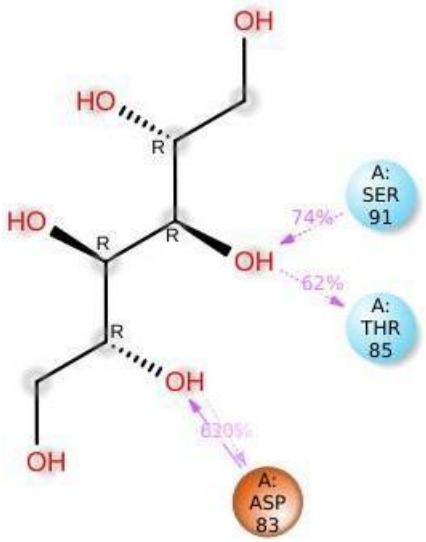

Figure 4.27. The interaction percentage of calcitonin amino acids with the D-mannitol

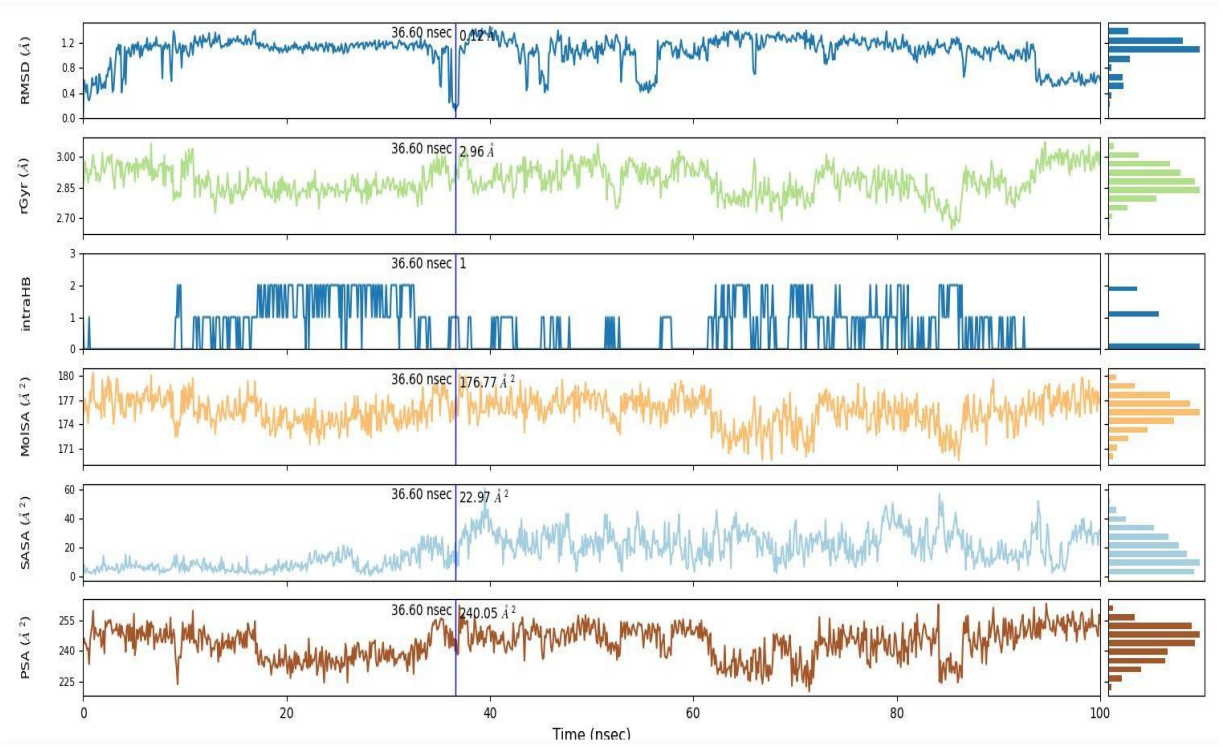

Figure 4.28: Ligand properties of D-mannitol such as radius of gyration (rGYr), intramolecular hydrogen bonding (Intra HB), molecular surface area (MolSA), solvent accessible surface area (SASA), and polar surface area (PSA).

In addition, RMSF analysis was conducted to evaluate the protein's flexibility (**Figure 4.25**). The Cα residues exhibited RMSF values within a limited range of 0.8 to 5.6 Å, suggesting no notable fluctuations. The protein's blue-α-helical and pink β-strands persisted over 50% of the simulation time, and the green line indicated the affinity between the protein and its ligand. The ligand contacting region was observed from 1.5 Å - 2.5 Å. D-mannitol formed strong hydrogen and hydrophobic interactions with the catalytic domain residues of the calcitonin hormone. Ligand RMSF depicted the interaction of ligand fragments with the protein, and 12 heavy atoms in D-mannitol were found to be present that interacted highly with the calcitonin hormone.

The histogram showed the number of amino acids interacting with D-mannitol, with the X-axis denoting amino acid position and the Y-axis denoting the interaction fraction scale. The interactions of hydrogen bonds are represented in green, hydrophobic bonds in lavender, and water bridges in blue are depicted in **Figure 4.26**. D-mannitol also interacted through the strong hydrogen bonds with the crucial amino acids in calcitonin hormone, such as ARG 58, CYS 81, ASP 83, ASP 84, THR 85, SER 91, TYR 92, GLN 93 of chain A and TYR 41, VAL 42, ARG 45, LYS 46 of chain B. Hydrophobic interactions are seen among the residues TRP 82 chain A, VAL 42, MET 49 of chain B. **Figure 4.27**. represents the interaction percentage of calcitonin amino acids of chain A: ASP 83 (62%), THR 85 (62%), SER 91 (74%) with D-mannitol. The potential ligand values (**Figure 4.28**) displayed several structural and surface properties that were analyzed, including RMSD, radius of gyration, molecular surface area (MolSA), solvent-accessible surface area (SASA), polar surface area (PSA), and intramolecular hydrogen bonds, and are expressed in Kcal/M, determining the protein-bound conformation of the ligand.

Molecular dynamics simulation (MDS) applies Newton's classical equations of motion to study protein-ligand interactions over time under defined conditions like temperature, pressure, volume, and density (Martinez, 2015). The best pose for each ligand is selected based on the highest dock score, indicating the most favorable binding energy. MDS analyzes the dynamic behavior of the docked pose of protein-ligand complex over time, indicating its stability, interactions, and binding free energy, which employs an effective drug design and optimization process. Root mean square deviations (RMSD), root mean square fluctuation (RMSF), radius of gyration (rGYr),

and number of hydrogen bonds (nHb) were the outcomes of MDS of protein-ligand docked complex (Noha *et al.,* 2017).

4.4.3 The Pharmacokinetic Parameters and Drug Likeness of the Identified Compounds.

The top 10 compounds from the SASM extract that exhibited a docking score of ≥3 kcal/M, with the calcitonin hormone, were selected to analyze their pharmacokinetic parameters using Swiss ADME. This evaluation includes physicochemical properties and Lipinski's five thumb rule (LVR5) filter analyses to assess the drug-likeness of these compounds, offering potential leads for further therapeutic exploration (Lipinski *et al.,* 1997). Throughout the years, numerous drug development failures have occurred due to poor pharmacokinetic characteristics, limited bioavailability, inefficacy, and high toxicity levels of the compounds (Daina and Zoete, 2016). The outcome of the drug design suite analysis revealed a desired pharmacokinetic profile of the tested compounds with optimal molecular weight. Lipophilicity and hydrogen bonding, predicting good absorption and bioavailability. The analysis further predicted ADMET properties, supporting the potential of these compounds.

In our results, **Table 4.12** represents that squalene and gamma-tocopherol violated the predicted Lipinski's Rule of Five values, likely due to their complex structures, high molecular weight, or excessive lipophilicity. Compounds violating two or more Lipinski parameters are generally considered likely to be orally inactive (Lipinski *et al.,* 1997). In contrast, the other compounds conformed to the standard range, aligning with the findings of Tijjani *et al.,* (2022), who reported that therapeutic agents with optimal hydrogen bond acceptors (HBA), hydrogen bond donors (HBD), and molecular weight (MW<500) exhibit favorable membrane permeability, drug-protein binding, distribution, and water solubility. According to Amir *et al.* (2024), 2-{5-[(2-hydroxyethyl)sulfanyl]-1,3,4-oxadiazol-2-yl}phenol conferred significant nephroprotection by enhancing antioxidant systems and mitigating renal injury, with pronounced effects observed at elevated doses. These results point to its potential use in preventing or treating kidney damage in the future.

Table 4.12. The physicochemical properties and lipophilicity of the top-hit compounds

Compounds	MV(g/M)	nHBD	nHBA	nRB	CLogP
D-mannitol	182.17	5	6	5	-2.23
Furyfurlmethylamphetamine	229.32	0	2	5	3.01
Nicotinic acid	123.11	1	3	1	0.32
Catechol	110.11	2	2	0	0.97
Squalene	410.72	0	0	15	9.38
Vanillin	152.15	1	3	2	1.20
Phthalic acid	166.13	2	4	2	0.84
Guanozole	99.09	3	2	0	-0.84
Maltol	126.11	1	3	0	0.55
Gamma tocopherol	416.18	1	2	12	7.83

Table 4.13: Solubility of the identified phytocompounds

Properties /Ligands	LogS (ESOL) Class	LogS (Ali) Class	LogS SILICOS- IT Class
D Mannitol	1.31 Highly soluble	1.12 Highly soluble	2.57 Soluble
Furfuryl methyl amphetamine	-3.46 Soluble	-3.27 Soluble	-5.10 Moderately soluble
Nicotinic acid	-1.26 Very soluble	-0.98 Very Soluble	-1.35 Soluble
Catechol	-1.63 Very Soluble	-1.31 Very soluble	-1.18 soluble
Squalene	-8.69 Poor Soluble	-11.57 In Soluble	-7.48 Poorly soluble
Vanillin	-1.82 Very soluble	-1.78 Very soluble	-1.88 soluble
Phthalic acid	-1.57 Very Soluble	-1.88 Very Soluble	-1.14 Soluble
Guanozole	-0.54 Very Soluble	-0.78 Very Soluble	-0.06 Soluble
Maltol	-1.17 Very soluble	-0.70 Very soluble	-1.71 Soluble
Gamma tocopherol	-8.29 Poorly soluble	-10.89 Insoluble	-8.79 Poorly soluble

Table 4.13 shows predicted aqueous solubility values (LogS) for various compounds using different models (ESOL, Ali, and SILICOS-IT). Most compounds, such as D-mannitol, Nicotinic acid, Catechol, Vanillin, Phthalic acid, Guanozole, and Maltol, exhibited good solubility across all models. However, compounds like Squalene and Gamma-tocopherol consistently showed poor solubility due to their high lipophilicity. Furfurylmethylamphetamine has varied predictions, with ESOL and Ali models indicating solubility and SILICOS-IT predicting moderate solubility.

Table 4.14: The pharmacokinetic parameters of the identified compounds

Properties									
Compounds	**GIA**	**BBB permeant**	**P-gp substrate**	**CYP1A2 inhibitor**	**CYP2C19 Inhibitor**	**CYP2C9 inhibitor**	**CYP2D6 inhibitor**	**CYP3A4 inhibitor**	**LogKp (cm/s)**
D-mannitol	Low	No	No	No	No	No	No	No	-9.61
Furyfurlmethy lamphetamine	High	Yes	No	No	No	No	Yes	No	-5.39
Nicotinic acid	High	Yes	No	No	No	No	No	No	-6.80
Catechol	High	Yes	No	No	No	No	No	Yes	-6.35
Squalene	Low	No	No	No	No	No	No	No	-0.58
Vanillin	High	Yes	No	No	No	No	No	No	-6.37
Pthallic acid	High	No	No	No	No	No	No	No	-6.80
Guanozole	High	No	No	No	No	No	No	No	-7.41
Maltol	High	Yes	No	No	No	No	No	No	-7.01
Gamma tocopherol	Low	No	Yes	No	No	No	No	No	-1.51

Table 4.14 summarizes the predicted pharmacokinetic profiles of the top 10 compounds, showcasing their distinct properties and potential implications for efficacy and safety. D-mannitol, Squalene, and Gamma-tocopherol showed low gastrointestinal absorption (GIA), while others like Nicotinic acid, Catechol, Vanillin, and Maltol had high GIA and blood-brain barrier (BBB) permeability. Furfurylmethyl amphetamine is notable for being a CYP2D6 inhibitor, and Catechol inhibits CYP3A4, suggesting potential drug interaction risks. Skin permeability ranged from poor (D-mannitol) to high (Squalene). These properties can impact the compounds'

therapeutic potential and safety profiles.

Table 4.15 depicts that the compounds exhibited varied toxicity profiles. Furfuryl methyl amphetamine and Catechol showed potential toxicity concerns, with high predicted values for acute toxicity, skin sensitization, and eye irritation. In contrast, D-mannitol and Vanillin appeared relatively safe, with low predicted toxicity values. Squalene and Gamma-tocopherol may pose skin-related toxicity risks due to high skin sensitization predictions. Toxicity profiles showed varying concerns, including hERG II inhibition (12.73%), AMES and liver toxicities (25.45%), and skin sensitivity (32.73%). However, many compounds demonstrated favorable pharmacokinetic properties, such as high Caco-2 and skin permeability, and blood-brain barrier penetration (Kalsoom *et al*., 2024).

Table 4.15: Toxicological properties of the identified phytocompounds

Toxicity						
Compounds	**hERG Blockers**	**Rat Oral Acute Toxicity**	**Skin sensitization**	**Carcino-genicity**	**Eye corrosion**	**Eye irritation**
D-mannitol	0.105	0.003	0.086	0.04	0.004	0.861
Furyfurlmethylamphetamine	0.111	0.905	0.437	0.508	0.935	0.649
Nicotinic acid	0.048	0.419	0.76	0.077	0.047	0.994
Catechol	0.005	0.898	0.933	0.726	0.983	0.991
Squalene	0.009	0.0	0.983	0.007	0.312	0.885
Vanillin	0.035	0.031	0.26	0.119	0.976	0.993
Phthalic acid	0.108	0.111	0.374	0.01	0.02	0.995
Guanozole	0.024	0.181	0.135	0.40	0.006	0.991
Maltol	0.054	0.33	0.548	0.788	0.545	0.943
Gamma-tocopherol	0.023	0.075	0.948	0.029	0.051	0.883

To enhance the potentiality of the phytocompounds, the absorption rate and druggability can be optimized through improved solubility, permeability, binding affinity, and ADME properties (Rudrapal *et al.,* 2022). A molecule's drug-likeness was indicated with minimal stars (0-5), showing higher drug-likeness. For successful drug development, strong binding of the ligand molecule to the target is essential for ensuring both oral bioavailability and the necessary drug-like properties (Daina *et al.*, 2017). Evaluating the physicochemical properties of these compounds is essential for

advancing drug development (Johnson and Wolfgang 2000).

A radar plot, or spider plot, effectively visualizes the ADMET properties of compounds during drug discovery. In **Figure 4.29**, the bioavailability radars showed that most predicted compounds exhibited favorable characteristics for oral bioavailability, including low flexibility and polarity, reduced toxicity, and good absorption. However, two compounds, squalene and gamma-tocopherol, are exceptions due to their poor solubility and skin-related toxicity.

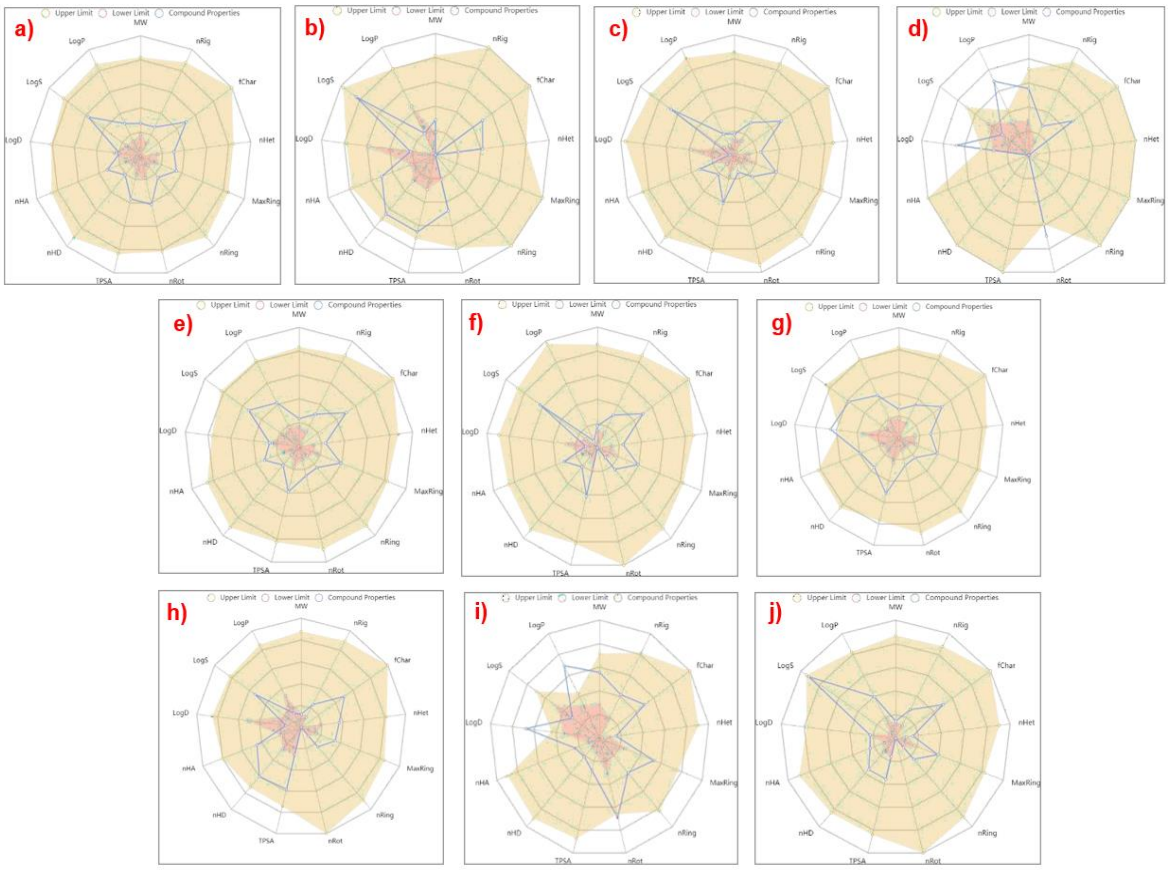

Figure 4.29. Radar plot showing the pharmacokinetic properties of phytocompounds

a) D-mannitol, b) Furfurylmethylamphetamine, c) Nicotinic acid, d) Catechol, e) Squalene, f) Vanillin, g) Phthalic acid, h) Guanozole, i) Maltol, j) Gamma tocopherol

All drug-likeness parameters fell within an acceptable range, suggesting favorable drug-like behavior for the phytocompounds. LogP, molecular weight (MW), and molecular polar surface area (PSA) indicated good membrane permeability,

intestinal absorption, and oral bioavailability. Meanwhile, parameters like the number of hydrogen bond acceptors (nHBAs), hydrogen bond donors (nHBDs), and rotatable bonds (nRotb) support drug metabolism and pharmacokinetics (DMPK). Some compounds exhibited higher lipophilicity, which may enhance their biological activity by improving the permeation and absorption through biological membranes (Rudrapal *et al.,* 2021). According to James *et al.* (2024), the compounds' physicochemical properties were within recommended ranges for molecular weight, volume, and polar surface area were within acceptable limits, except for xanosporic acid, which violated two of Lipinski's Rules of Five, potentially affecting its oral bioavailability.

In Phase IV, molecular docking studies identified D-mannitol as a potential antagonist, showing high binding affinity to Tamm-Horsfall protein, Calcium oxidoreductase enzyme, and Calcitonin hormone. Molecular dynamics simulation confirmed D-mannitol's stable interaction with Calcitonin, forming strong hydrogen bonds and hydrophobic interactions. Pharmacokinetic analysis showed that most compounds, including D-mannitol, had favorable profiles, with good solubility, absorption, and bioavailability. However, some compounds like Squalene and Gamma-tocopherol exhibited poor solubility and potential toxicity concerns. Overall, the study suggests the therapeutic potential of SASM extract in preventing and treating urolithiasis, which implies that the extract may offer an effective herbal remedy for kidney stone recurrence, reducing pain and discomfort. The findings of this study assist in future research on *S. articularis* to explore the mechanism of action and drug development.